

USA PASSION DEVELOPMENT CONFERENCE PROCEEDING

EISBN: 978-967-16483-1-5

The 1st International Conference of Applied Biology, Chemistry & Science (ICABCS 2018)



**The 1st International Conference of Applied Biology, Chemistry
& Science (ICABCS 2018)**

**27-28 October 2018,
Equatorial Hotel Malacca, Malaysia**

Copyright © 2018

USA Passion Development Sdn Bhd (1279049-D)

**805B, 2nd Floor Complex Diamond, Bangi Business Park (Jalan Medan Bangi
Off Persiaran Bandar) 43650 Bandar Baru Bangi, Selangor, Malaysia**

**All rights reserved. No part of this proceeding may be reproduced or
transmitted in any form or by any process without the prior written
permission of the publisher, except for the inclusion of brief quotations for
Review.**

E-ISBN : 978-967-16483-1-5

EDITORIAL BOARD

EDITOR IN CHIEF

Prof. Dato' Sri Dr. Ashgar Ali bin Ali Mohamed

Universiti Islam Antarabangsa Malaysia (International Islamic University of Malaysia)

EDITOR

Assoc. Prof. Dr. Mohd. Faizal Mohd Isa

Universiti Utara Malaysia (North University of Malaysia)

CO-EDITOR

Dr. Zul Ariff Bin Abdul Latiff

Universiti Malaysia Kelantan (University of Kelantan Malaysia)

CO-EDITOR

Ts. Dr. Nor Haslinda Binti Abas

Universiti Tun Hussein Onn Malaysia (University of Tun Hussein Onn Malaysia)

MANAGING EDITOR

Mr. Muhammad Aidil Bin A Raof

USA Passion Development Sdn. Bhd.

CONTENTS

TITLE	PAGE
PHENANTHRENE BIODEGRADATION EFFICIENCY OF BACILLUS SP. P4A ISOLATED FROM HYDROCARBON CONTAMINATED SOIL By Fazilah Ariffin, Noraznawati Ismail, Darah Ibrahim	5
THE SAFETY OF MIXED EXTRACTS OF PIPER ADUNCUM FRUIT AND TEPHROSIA VOGELII LEAF AGAINST PARASITIOD DIADEGMA SEMICLAUSUM By Dr. Eka Candra Lina, SP, MSi., SisriMarleni., Dr. Ir. Nurbailis, MS., Prof. Dr. Novri Nelly MS.	11
REGENERATED KENAF CORE CELLULOSE PRODUCTS PREPARED VIA PRE-COOLED METHOD By Hatika Kaco, Mohd Shaiful Sajab, Sarani Zakaria, Chin Hua Chia	15
CLASSIFICATION OF CANCER GENE SUBTYPES FROM CLUSTERING OF GENE EXPRESSION DATA By Logenthiran Machap, Afnizanfaizal Abdullah, Zuraini Ali Shah	21
THE SYNERGISTIC ANTIBACTERIAL EFFECTS OF CINNAMOMUM VERUM AND CYMBOPOGON CITRATES ON URINARY TRACT INFECTIONS CAUSING PATHOGENS ESCHERICHIA COLI AND PSEUDOMONAS AERUGINOSA By Fional Lawing, Noor Faradilla Abdullah, Che Wan Imanina Che Wan Takwa	26
DENSIFICATION BEHAVIOR AND MECHANICAL PROPERTIES OF CERIUM OXIDE AND MANGANESE OXIDE-DOPED YTTRIA TETRAGONAL ZIRCONIA POLYCRYSTALS CERAMICS FOR DENTAL APPLICATIONS. By G. Sankar, S. Meenaloshini, R. Dinesh	30
EFFECT OF CEO ₂ AND MNO ₂ ON THE MICROSTRUCTURE, DEGRADABILITY AND MECHANICAL PROPERTIES OF ZIRCONIA By D. Ragurajana, M. Satgunama, U. Sankara, M. Golieskardia	33

LINEAR HYBRID CELLULAR AUTOMATA (LHCA) RULE 90/150 BASED
S-BOX

36

By Muhammad Fahim Roslan, Kamaruzzaman Seman, Azni Haslizan Ab
Halim, M Norazizi Md Sayuti

PHENANTHRENE BIODEGRADATION EFFICIENCY OF *BACILLUS* SP. P4A ISOLATED FROM HYDROCARBON CONTAMINATED SOIL

Fazilah Ariffin^{*1}, Noraznawati Ismail², Darah Ibrahim³

^{*1}School of Fundamental Science, Universiti Malaysia Terengganu, Malaysia

²Institute of Marine Biotechnology, Universiti Malaysia Terengganu, Malaysia

³Industrial Biotechnology Research Laboratory (IBRL), School of Biological Sciences, Universiti Sains Malaysia, 11800 Minden, Penang, Malaysia

Abstract: In this study, phenanthrene-degrading bacteria was successfully isolated from hydrocarbon contaminated soil. The bacteria were identified based on their morphological, biochemical activities and molecular identification using 16S rRNA. The phenanthrene – degrading capabilities was cultivated in an enrichment culture containing phenanthrene as a sole source of carbon and energy. The phenanthrene degradation was analysed using Gas Chromatography-Flame Ionization Detector (GC-FID) and the result obtained indicated that the *Bacillus* sp. P4a was capable of degrading to about 83.01% in the enrichment culture. The *Bacillus* sp. P4a has been shown to degrade phenanthrene via salicylate pathway which produced salicylic acid and catechol compound after 14 and 28 days of incubation. The result revealed that this bacterial isolate can be highly recommended for bioremediation of hydrocarbon contaminants due to their capability to degrade phenanthrene.

Keywords: Phenanthrene, Bacillus sp. P4a, Biodegradation, Bioremediation, Contaminated soil

INTRODUCTION

In recent decades, the contamination of soil by pollutant such as polycyclic aromatic hydrocarbon (PAH) has caused serious concerns. PAHs have a widespread occurrence in various ecosystems which enable them to persist for a long time in the environment (El-Shahawi et al., 2010). Due to its toxic, mutagenic and carcinogenic properties, prolonged exposure to a high concentration of PAHs can cause acute and chronic health problems (Kim et al., 2013). Thus, bioremediation is a technique created to remediate the PAH contamination to reduce the negative impacts of the PAH. It is widely used to remove PAHs from the environment since it is cost effective and environmentally friendly compared to other conventional methods.

OBJECTIVE

The objective of the present study is to determine the biodegradation capability of the bacterial isolate using a shake flask system. It is also to determine the involvement of intermediates during the phenanthrene degradation process in the liquid system.

LITERATURE REVIEW

The presence of PAH pollutant creates harm to the environment and human because of their toxic and carcinogenic characteristics (Laws, 2013). There were 67 PAH compound showed mutagenic properties to human (Durant et al., 1996). Some of the PAH exposure may disturb our respiratory and gastrointestinal tract and also the skin (Ramesh et al., 2004). It also interferes with other life environment such as aquatic organisms through pollution in the food chain. It is harmful to human due to the consumption of this contaminated seafood.

Phenanthrene is a low molecular weight PAH which consists of three fused benzene rings with phenyl and anthracene compound attached together. It is toxic pollutant and occurs as a major component of PAH compounds in the environment (Slezakova *et al.*, 2013). Therefore, biodegradation of this compound need to be done in order to bioremediate the contaminated soils.

Several bacterial strains have been shown to degrade phenanthrene such as *Arthrobacter* sp., *Acidovorax* sp., *Brevibacterium* sp., *Burkholderia* sp., *Comamonas* sp., *Mycobacterium* sp., *Pseudomonas* sp. and *Sphingomonas* sp. (Seo *et al.*, 2009). These bacteria have the capability to degrade phenanthrene and utilize it as a nutrient source (Seo *et al.*, 2009). Some of the bacteria from genus *Mycobacterium* have been demonstrated to metabolize phenanthrene using both enzymes dioxygenase and monooxygenase to react on the aromatic compound (Seo *et al.*, 2012).

METHODOLOGY

Sample Collection

The soil samples obtained near a palm oil mill factory were collected using clean stainless steel spatula and stored in sterile plastic bags before being transferred to the laboratory. The samples were stored at 4°C before analysis.

Enrichment and Isolation of Phenanthrene-degrading bacteria

The phenanthrene-degrading bacteria were enriched in flasks containing 150 ml of Minimal Salt Medium (MSM), 15 g of soil sample and 5 ml of phenanthrene (330 mg/l). The MSM contained (g/L): 1.0 g (NH₄)₂SO₄, 0.1 g CaCl₂·2H₂O, 0.8 g K₂HPO₄, 0.2g KH₂PO₄, 0.012g FeSO₄·7H₂O, 0.003 g MnSO₄·7H₂O, 0.003 g ZnSO₄·7H₂O in 1 Liter of distilled water (modified from Coral & Karagoz, 2005). The flasks were incubated at 30°C with 150 rpm. Then, 5 ml aliquots were transferred to a new MSM containing 5 ml of phenanthrene. The flasks were shaken for 14 days. Bacteria were isolated by the serial where 0.1 ml from the series of dilution was spread onto the nutrient agar (NA) plates and incubated at 30°C for 48 hours.

Identification of the selected phenanthrene-degrading bacterial isolate

The identification and characterization of selected bacterial isolates were based on macroscopic and microscopic observations. The morphology of the bacterial isolates was observed using the Gram staining technique. The physiological characterization of the bacteria was performed using standard biochemical tests of the BBL Crystal Identification Kit (Jackson *et al.*, 2004). The bacterial isolates were further characterized at the molecular level of DNA sequencing analysis of 16S rRNA.

Phenanthrene degradation analysis by locally isolated bacteria

The analysis of phenanthrene concentration in the culture medium was conducted at the regular interval every 4 days. Duplicated bacterial cultures were centrifuged at 5000 rpm for 10 minutes and at 4°C. The layer of the obtained supernatant was mixed with 100 ml of hexane in 250 ml separation funnel and vigorously shake. There were two layers or phases formed in the separation funnel. The extraction was repeated three times and the hexane phase (top layer) was separated and pooled in a beaker. Then, it was air dried in a fume hood. When the analysis was to be carried out, the samples were then dissolved with an equal volume of hexane (100 ml) and the phenanthrene was quantified by a Clarus 500 Gas Chromatography-Flame Ionization Detector (GC-FID).

Identification of phenanthrene metabolites

An analysis of phenanthrene metabolites (Mallick *et al.*, 2007) in the culture medium was conducted at Day 0, Day 14 and Day 28 of incubation. The cells were removed by centrifugation at 5000 rpm for 10 minutes and 4°C. The supernatants obtained were membrane-filtered and acidified to pH 2. The supernatant were extracted with three volumes of 100 ml ethyl acetate. The organic extracts were pooled and concentrated to 10 ml using rotavapour unit (Buchi, Germany). The extracts were air dried and stored at room temperature until further analysis. The residue was then dissolved in 1 ml of methanol and analysed using Gas Chromatography-Mass Spectrometry (GC-MS Agilent 6890N/59731).

FINDINGS

Identification of phenanthrene-degrading bacteria

The morphology of the potential phenanthrene-degrading bacterial was observed using the Gram staining method. It was shown that the Isolate P4a is Gram-positive rod-shaped bacteria. It was produced a white colony possessed a dry surface, a filamentous form of the colony, flat elevation and filiform margin. The identification that based on a biochemical test and BBL Crystal Identification Kit showed that Isolate P4a was preliminarily identified as *Bacillus* sp. The molecular approach such as 16S rRNA gene analysis of Isolate P4a was carried out using genomic extraction, PCR and sequencing. The sequence showed 99% of the *Bacillus* sp. N30 identity respectively. *Bacillus* sp. was the most widely reported phenanthrene degraders isolated from the environment (Patel *et al.*, 2013).

Degradation activity of phenanthrene by *Bacillus* sp. P4a

There was about 83.00% of phenanthrene degradation throughout the 28 days incubation. The degradation was analyzed using GC-FID to measure the decrease in the peak area of phenanthrene. Concomitant phenanthrene degradation with the growth of bacteria can be observed (Figure 1). The bacteria count increases from Log CFU/ml 4.10 at day 0 to Log CFU/ml 5.67 after 8 days of cultivation. Referring to Figure 1a, it shows that the bacteria grow in the log phases on the first day of cultivation up to 8 days after inoculation. This condition suggests that the bacteria have been previously exposed to PAH particularly during the isolation and screening processes. Once the bacteria have adapted to the new medium, they begin to reproduce and multiply their numbers for each increment of time. However, the bacterial growth steady has shown a decrease from Log CFU/mL 5.67 at day 8 to Log CFU/mL 3.27 at day 28 of cultivation This is supported by the finding of Zhao *et al.* (2017) where the bacterial reproduction and growth regularly reduced because the carbon and nutrient sources have been used by the bacteria in the cultivation medium. By the end of the cultivation period, the bacterial growth entered the final growth phase which nutrients have been depleted and cell number decreases. The phenanthrene degradation activity is different from one species to another. Referring to Ling *et al.* (2011), *Bacillus* sp. could utilize various PAH such as phenanthrene as a sole source of carbon.

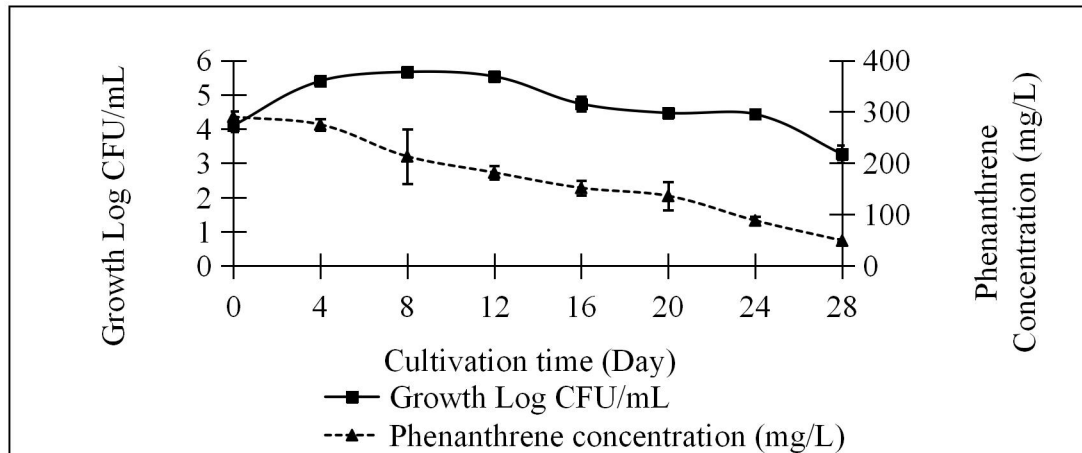


Figure. 1: Profile of viable cell count and phenanthrene concentration(mg/L) in flask system containing *Bacillus* sp. P4a

Metabolites production in phenanthrene degradation by *Bacillus* sp. P4a

In the present study, there were three metabolites identified by GC-MS from the organic extracts of *Bacillus* sp. The P4a culture containing phenanthrene was incubated at Day 0, Day 14 and Day 28 (Table 1). The metabolites obtained correspond with 1-naphthalenecarboxylic acid, salicylic acid and catechol, respectively (Figure 2).

Table 1

GC-MS data for metabolites of phenanthrene obtained from organic extract of *Bacillus* sp. P4a culture

Incubation (Day)	Metabolites	Retention time (min)	m/z of fragment ions % Relative Intensity	Possible structure
0	A	10.7	184 (16, M ⁺), 155 (100, 140 (4), 127 (70), 113 (3), 101 (6), 87 (5), 77 (12), 63 (19), 51 (11), 27 (2)	1-Napthalene carboxylic acid
14	B	9.73	138 (17,M ⁺), 121 (100), 109 (2), 93 (23), 81 (3), 65 (25), 53 (5), 39 (82), 27 (2)	Salicylic acid
28	C	8.95	126 (2, M ⁺), 124 (100), 107 (12), 95 (7), 78 (48), 62 (7), 51 (19), 39 (18), 27 (5)	Catechol

Zhao, H., Zhang, Y., Xiao, X., Li, G., Zhao, Y., & Liang, Y. 2017, Different phenanthrene-degrading bacteria cultured by in situ soil substrate membrane system and traditional cultivation. *International Biodeterioration & Biodegradation*, 117, 269-277

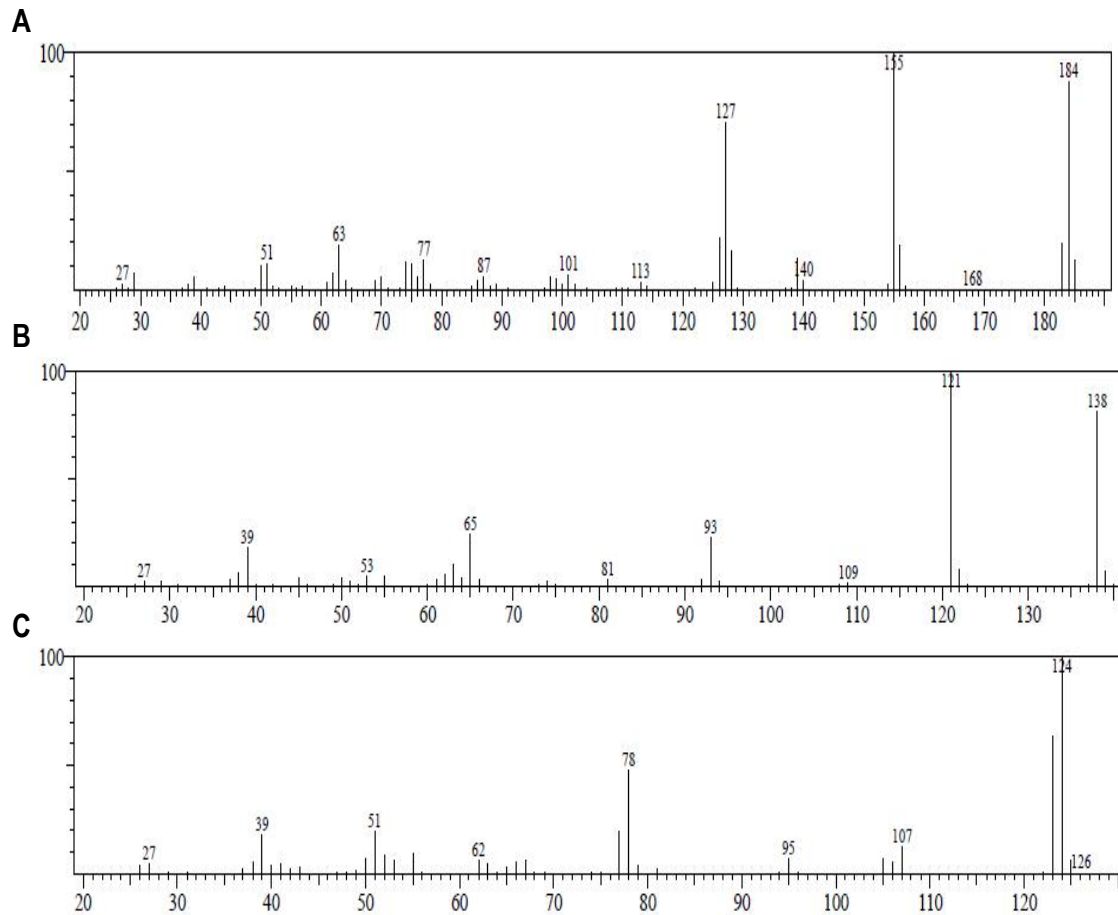


Figure. 2: Mass spectral profiles of phenanthrene metabolites produced by *Bacillus* sp. P4a, (A) 1-Naphthalenecarboxylic acid (B) salicylic acid and (C) catechol.

CONCLUSION

Bacillus sp. P4a showed the capability in degrading phenanthrene which was 83.01% at 28 days of incubation. It has been shown to degrade phenanthrene via salicylate pathway which produced salicylic acid and catechol compound after 14 and 28 days of incubation. Thus *Bacillus* sp. P4a gave a great potential to be applied in bioremediation of environments polluted by phenanthrene. These potential bacterial culture can be highly recommended for bioremediation of hydrocarbon contaminants due to their capability to degrade phenanthrene

MAIN REFERENCES

- Coral, G., & Karagoz, S. 2005, Isolation and characterization of phenanthrene-degrading bacteria from a petroleum refinery soil. *Annals of microbiology*, 55(4), 255.
- Durant, J. L., Busby Jr, W. F., Lafleur, A. L., Penman, B. W., & Crespi, C. L. 1996, Human cell mutagenicity of oxygenated, nitrated and unsubstituted polycyclic aromatic hydrocarbons associated with urban aerosols. *Mutation Research/Genetic Toxicology*, 371 (3–4), 123-157.
- El-Shahawi, M. S., Hamza, A., Bashammakh, A. S., & Al-Saggaf, W. T. 2010, An overview on the accumulation, distribution, transformations, toxicity and analytical methods for the monitoring of persistent organic pollutants. *Talanta*, 80(5), 1587-1597.
- Jackson, C. R., Fedorka-Cray, P. J., & Barrett, J. B. 2004, Use of a Genus- and Species-Specific Multiplex PCR for Identification of Enterococci. *Journal of Clinical Microbiology*, 42 (8), 3558-3565.
- Kim, K. H., Jahan, S. A., Kabir, E., & Brown, R. J. 2013, A review of airborne polycyclic aromatic hydrocarbons (PAHs) and their human health effects. *Environment International*, 60, 71-80.
- Laws, E. A. 2013, Environmental Toxicology, Introduction. In: *Environmental Toxicology*. Springer, New York. pp. 1-15.
- Ling, J., Zhang, G., Sun, H., Fan, Y., Ju, J., & Zhang, C. 2011, Isolation and characterization of a novel pyrene-degrading *Bacillus vallismortis* strain JY3A. *Science of the Total Environment*, 409 (10), 1994-2000.
- Mallick, S., Chatterjee, S., & Dutta, T. K. 2007, A novel degradation pathway in the assimilation of phenanthrene by *Staphylococcus* sp. strain PN/Y via meta-cleavage of 2-hydroxy-1-naphthoic acid: formation of trans-2,3-dioxo-5-(2'-hydroxyphenyl)-pent-4-enoic acid. *Microbiology*, 153(7), 2104-2115.
- Patel, V., Patel, J., & Madamwar, D. 2013, Biodegradation of phenanthrene in bioaugmented microcosm by consortium ASP developed from coastal sediment of Alang-Sosiya ship breaking yard. *Marine Pollution Bulletin*, 74 (1), 199-207.
- Ramesh, A., Walker, S. A., Hood, D. B., Guillén, M. D., Schneider, K., & Weyand, E. H. 2004, Bioavailability and risk assessment of orally ingested polycyclic aromatic hydrocarbons. *International Journal of Toxicology*, 23 (5), 301-333.
- Slezakova, K., Pires, J. C. M., Castro, D., Alvim-Ferraz, M. C. M., Delerue-Matos, C., Morais, S., & Pereira, M. C. 2013, PAH air pollution at a Portuguese urban area: carcinogenic risks and sources identification. *Environmental Science and Pollution Research*, 20 (6), 3932-3945
- Seo, J.-S., Keum, Y.-S., & Li, Q. 2009, Bacterial Degradation of Aromatic Compounds. *International Journal of Environmental Research and Public Health*, 6 (1), 278-309
- Seo, J.-S., Keum, Y.-S., & Li, Q. X. 2012, *Mycobacterium aromativorans* JS19b1T degrades phenanthrene through C-1, 2, C-3, 4 and C-9, 10 dioxygenation pathways. *International Biodeterioration & Biodegradation*, 70 (0), 96-103

THE SAFETY OF MIXED EXTRACTS OF *Piper aduncum* FRUIT AND *Tephrosia vogelii* LEAF AGAINST PARASITIOD *Diadegma semiclausum*

Dr. Eka Candra Lina¹, SP, MSi¹., SisriMarleni¹., Dr. Ir. Nurbailis, MS¹., Prof. Dr. Novri Nelly MS¹.

¹Faculty of Agricultural, Universitas Andalas, Limau Manis, Padang, Sumatera Barat

Abstract: The mixed *Piper aduncum* fruit and *Tephrosia vogelii* leaf extracts processed to form *emulsifiable concentrates* (EC) or *wettable powder* (WP) that actively control the cabbage pest *Plutella xylostella*. The objective of this study was to determine the effect of EC and WP formulations on the parasitoid *Diadegma semiclausum*. Their effects on parasitoid *D. semiclausum* can be seen from the mortality, life time, parasitization ability, and *sex ratio* of the parasitoid. Completely randomized design was used with 4 treatments and 6 replications. The thin layer residue method was used with EC and WP at twice the LC₉₅ value determined for *P. xylostella* (appropriate controls were used). The EC and WP formulations had not effect on the mortality, the life time, parasitization ability or the *sex ratio* of the parasitoid *D. semiclausum*. These EC and WP formulations can be used to control the cabbage pest *P. xylostella* in field related to an integrated pest management system.

Keyword: *Botanical insecticide, emulsifiable concentrate* (EC), *wettable powder* (WP), *Diadegma semiclausum*

INTRODUCTION

Leaf caterpillar *Plutella xylostella* is one of the main pests in cabbage plants caused 50-100% yield loss without control effort (Winarto and Nazir, 2004). The presence of natural enemy decrease attack rate of *P. xylostella* 71% - 82%. Unfortunately the population of natural enemy parasitoid *D. semiclausum* significantly decrease due to intensive use of synthetic insecticides (Mukholifah *et al.*, 2014).

All problems above meet to environmental friendly control technique called botanical insecticides. Lina *et al.*, (2014) develop formulations of mixture *T. vogelii* leaf and *P. aduncum* fruit (1:5). Formulations were strong synergistic action against *C. pavonana* and were safe against its natural enemies *Eriborus argenteopilosus*. Both formulations do not cause phytotoxic symptoms in broccoli plants. Lina *et al.*, (2018) determine the same formulations killed another main pest of cabbage plant *Plutella xylostella*. The values of LC₉₅ EC and WP formulations were 0.35 % and 0.37% respectively. The safety of formulations against natural enemies. Of *P. xylostella*, parasitoid *D. semiclausum* was

The purposes of this research to determine the effect of *emulsifiable concentrates* (EC) or *wettable powder* (WP) formulations of mixed *Piper aduncum* fruit and *Tephrosia vogelii* leaf extracts on the mortality, life time, parasitization ability or the *sex ratio* of the parasitoid *D. semiclausum*.

METHODOLOGY

This research conducted at the Insect Bioecology Laboratory and wirehouse of Plant Pests and Diseases Department, Faculty of Agriculture, Andalas University, Padang from August to October 2017.

Botanical insecticides formulations from mixture extract of *P. aduncum* fruit and *T. vogelii* leaf in the form of formulations *emulsifiable concentrate* (EC) and *wettable powder* (WP) were tested at concentration $2 \times LC_{95}$ against parasitoid *D. Semiclausum*. Preparation of formulations refer to Lina (2014). Determination of concentration was obtained from previous research which had been carried out by Lina *et al.*, (2018). Thin layer residues method on the surface of the test tube used to examine formulations safety against parasitoid *D. semiclausum*. Mortality and *sex ratio* data of parasitoid *D. semiclausum* were observed, while the data of life time and parasitization ability of parasitoid *D. semiclausum* were analyzed by variance (Test F) at 5% significance level and continue with *Least Significant Different* (LSD) at the 5%.

FINDING

A. Mortality imago *Diadegma semiclausum*

Mixture extract of *P. aduncum* fruit and *T. vogelii* leaves in form EC and WP Formulations at a concentration $2 \times LC_{95}$ did not cause mortality of male and female of *D. semiclausum* parasitoid at 24 hours after treatment compare to control.

Table 1. Imago mortality *D. semiclausum* at a concentration of $2 \times LC_{95}$ EC and WP formulation

Treatment	Number of individuals	Mortality (%)	
		Male	Female
EC Control	6	0	0
WP Control	6	0	0
$2 \times LC_{95}$ EC	6	0	0
$2 \times LC_{95}$ WP	6	0	0

Life time of male and female of parasitoid *D. semiclausum* after treated with EC and WP formulations of mixture extract from *T. vogelii* and *P. aduncum* can be seen on Table 2. There is no significant different ($P_{\text{male}} = 0.9805$ and $P_{\text{female}} = 0.9818$) between the life time of treated parasitoid and control.

Table 2. The average of Life Time imago *D. semiclausum* after treated with botanical insecticides in the form of EC and WP formulations

Treatment	Life Time imago <i>D. semiclausum</i> (X ± SD) (Day)	
	Male	Female
EC Control	6,00 ± 3,40	6,16 ± 3,65
WP Control	6,00 ± 1,54	6,00 ± 1,54
2×LC ₉₅ EC	5,83 ± 3,76	6,33 ± 3,66
2×LC ₉₅ WP	6,50 ± 2,34	6,66 ± 2,25

C. Parasitization ability of *Diadegma semiclausum*

The ability of parasitization of *D. semiclausum* to larvae *P. xylostella* was not significantly different ($P = 0.9814$) between control of EC and WP formulations and treatment of EC and WP formulation. The average ability of parasitization of parasitoid *D. semiclausum* can be seen from the number of parasitic pupae that appear from parasitized larvae (Table 3).

Table 3. Average number of pupae parasitized by female imago *D. semiclausum* after treatment of Botanical insecticides in the form of EC and WP formulation

Treatment	Number of parasitic pupae (X ± SD)
EC Control	28,00 ± 22,04
WP Control	30,33 ± 8,64
2×LC ₉₅ EC	26,50 ± 21,54
2×LC ₉₅ WP	29,16 ± 9,74

Table 4. Comparison of male and female imago (*sex ratio*) generated by imago *D. semiclausum*

Treatment	Male : Female
EC Control	3 : 2
WP Control	2 : 1
2×LC ₉₅ EC	3 : 2
2×LC ₉₅ WP	3 : 2

CONCLUSION

EC and WP formulations mixed fruit extract *Piper aduncum* and leaves *Tephrosia vogelii* with a concentration of $2 \times LC_{95}$ safe against parasitoid *D. semiclausum*. This is indicated by the absence of influence on life duration, parasitization ability and sex ratio and 0% mortality of parasitoid *D. semiclausum*.

MAIN REFERENCES

- Lina, E.C., Dadang., S. Manuwoto., dan G. Syahbirin. 2013. Synergistic action of mixed extracts of *Brucea javanica* (Simaroubaceae), *Piper aduncum* (Piperaceae), and *Tephrosia vogelii* (Leguminosae) against cabbage head caterpillar, *Crociodolomia pavonana*. Journal of Biopesticides.
- Lina, EC., I. Widhianingrum, M.E. Putri, N.A Evalia, M. Makky. 2018. Insecticidal activity of Piper aduncum fruit and Tephrosia vogelii leaf mixed formulations against *Plutella xylostella* (L.) (Lepidoptera: Plutellidae). Jbiopest 11(1) : 69-75.
- Maulina, F. dan Muflihayati. 2013. Conservation of *Diadegma semiclausum* Hellen. Parasitoids as biological control to *Plutella xylostella* Linn. With adult food exploration. International journal on advanced science engineering information technology. 3 (5) : 2088 – 5334.
- Wardani, N., dan Nazar, A. 2002. Evaluasi Tingkat Parasitisasi Parasitoid Telur dan Larva Terhadap *Plutella xylostella* L. (Lepidoptera: Yponomeutidae) pada tanaman kubis-kubisan. J.HPTT 2(2): 55.
- Winarto, L., dan D. Nazir. 2004. Teknologi Pengendalian Hama *Plutella xylostella* dengan Insektisida dan Agen Hayati Pada Kubis Di Kabupaten Karo. Jurnal Pengkajian dan Pengembangan Teknologi Pertanian 7 : 1 : 27 -33.
- Zarkani, A., D. Prijono., dan Putjianto. 2009. Efektivitas ekstrak *Piper retrofractum* dan *Tephrosia vogelii* dan campuran terhadap *Crociodolomia pavonana* dan *Plutella xylostella* serta keamanan ekstrak tersebut terhadap *Diadegma semiclausum*. Jurnal Akta Agrosia 12:1:35 – 44.



REGENERATED KENAF CORE CELLULOSE PRODUCTS PREPARED VIA PRE-COOLED METHOD

Hatika Kaco^{1*}, Mohd Shaiful Sajab², Sarani Zakaria³, Chin Hua Chia³

¹ Kolej PERMATA Insan, Universiti Sains Islam Malaysia, Bandar Baru Nilai,

71800 Nilai, Negeri Sembilan, MALAYSIA.

² Research Center for Sustainable Process Technology (CESPRO), Faculty of Engineering and Built Environment, Universiti Kebangsaan Malaysia, 43600 UKM Bangi, Selangor, MALAYSIA.

³ Bioresources and Biorefinery Laboratory, Faculty of Science and Technology,

Universiti Kebangsaan Malaysia, 43600 UKM Bangi, Selangor, MALAYSIA.

ABSTRACT

Cellulose was prepared from kenaf core (KC) powder by a series of bleaching and alkali treatment processes. The extracted cellulose was dissolved using different the alkali/urea solvents (NaOH/urea and LiOH/urea) via pre-cooled method to form cellulose solution. Cellulose solution produced from KC cellulose was regenerated to form cellulose hydrogel. Hydrogel produced from cellulose with lower cellulose content possessed higher porosity, hence increased the water swelling of the hydrogel. Cellulose solution also was mixed at different percentage of polyvinyl alcohol (PVA) to produce regenerated transparent membranes. The addition of 10 % of PVA has increased the porosity of the regenerated membrane. The regenerated cellulose/PVA membranes were color-printed using a laser printer and the membranes were recycled, in which the printed ink was removed using distilled water and printed repeatedly for several times. Crosslinking of the KC cellulose solution with aldehyde based crosslinker (glyoxal and glutaraldehyde (GA)) were studied using different percentages of the aldehyde. Tensile strength of the membranes increased with increasing crosslinker percentages. However, the porosity decreased due to the crosslinked cellulose structure. Moreover, magnetite (Fe_3O_4) nanoparticles was synthesised and were embedded in cellulose solution for the preparation of magnetic cellulose membrane (MCM). The formed cellulose solution was mixed with Fe_3O_4 nanoparticle at different percentage of Fe_3O_4 i.e., 10, 20 and 30 % to produce regenerated MCM. From XRD result, it shows that the CrI of cellulose decreased with the addition of magnetite nanoparticles. However, it is obtained from VSM test that the magnetic properties of the regenerated membrane increases as the percentages of magnetite nanoparticle increases.

Keywords: Cellulose hydrogel; cellulose membrane; crosslinking; kenaf cellulose; pre-cooled method

INTRODUCTION

Kenaf is one of the important industrial crops cultivated in Malaysia after wood and bamboo (Mohd Edeerozey et al. 2007). Recently, various studies have been reported in utilizing kenaf for different applications due to its advantages such as renewable resources, fast growing rate, and annually available. Kenaf core with shorter fiber length are less used compare to kenaf bast which gives advantages to the pre-cooled system using alkali/urea solvent. This will ease the cellulose dissolution to be occurred. Alkali/urea system is used due to the green process which promises non-toxic process, cheaper, biodegradable and rapid dissolution process (Zhang et al. 2010). The produced regenerated cellulose products were used in the form of fibers, films, powders, beads, and membranes. The cellulose morphology changes after dissolution and regeneration process occurred where the processes have affected the properties of the regenerated cellulose produced.

In this study, cellulose was isolated from kenaf core powder undergoes bleaching and alkali treatment. The extracted cellulose was dissolved in LiOH/urea solvents. Cellulose hydrogel was produced using different cellulose content. Regenerated cellulose membrane was mixed with PVA solution to form transparent and printable membrane. Crosslinked cellulose membrane with aldehyde based (glutaraldehyde and glyoxal) were produced to study crosslinking effect on chemical, physical and mechanical properties of the membrane. Magnetite was synthesized using in-situ method and cellulose was dissolved in NaOH/urea solvent to produce cellulose solution for the production of magnetite cellulose membrane (MCM) at different magnetite content. The properties of hydrogel and membranes produced were characterized using UV-Vis, SEM, FTIR and XRD. Water uptake of both hydrogel and crosslinked membrane was also investigated.

METHODOLOGY

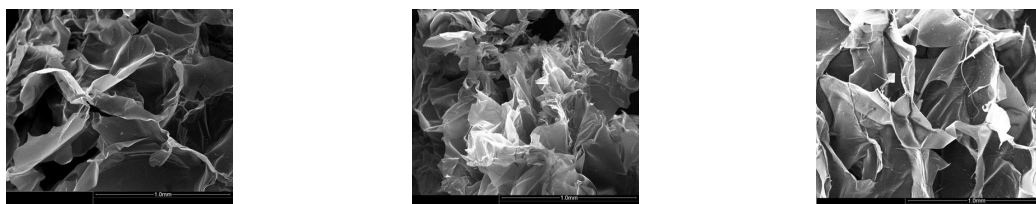
Kenaf cellulose (KC) (3 wt %) were dissolved in LiOH/urea aqueous solution and frozen at -13°C . Then, ECH (5 %) was dropped wisely into the cellulose solution and stirred until the formation of hydrogel achieved. Cellulose/polyvinyl alcohol (CS/PVA) solutions were prepared in different ratios of PVA and CS. The CS/PVA solution was stirred for 30 min and centrifuged and cast on a glass plate and coagulated in 5% H_2SO_4 solution to form the CS/PVA film. Two different types of crosslinker (glutaraldehyde (GA) and glyoxal) were used as coagulant and prepared at different percentages of crosslinker. The prepared CS was cast on a glass plate and immersed in different coagulating baths. The crosslinked membrane produced were freeze dried and air dried for further characterization.

Magnetite nanoparticles were synthesis by using of Fe(II), Fe(III) and NaOH dissolved in distilled water at 50 to 60 $^{\circ}\text{C}$. The solution turned black color after the addition of NaOH which indicates the formation of magnetite. To form magnetite cellulose membrane (MCM), the synthesized magnetite was added into the cellulose solution at different magnetite content (10, 20 and 30 %) and stirred homogeneously, cast on a glass plate and coagulated in acid bath to form MCM.

RESULTS AND DISCUSSION

Production of Cellulose Hydrogel

Figure 1 shows the SEM images of hydrogel prepared using different percentage of cellulose. The sample coded as HKCR2, HKCR3 and HKCR3.5 represent the 2 %, 3 % and 3.5 % of KCR cellulose dissolved in LiOH/urea solvent to form hydrogel respectively. It shows clearly that by increasing the cellulose content from 2 to 3.5 %, the average pore size of the hydrogel has decreased. This may be due to the entanglement between the cellulose chain is greater at higher cellulose content (Chang et al. 2010).



(a) (b) (c)
 Figure 1 SEM images of the cross-sections of the hydrogels (a) HKCR2 (b) HKCR3 and (c) HKCR3.5

Figure 2 shows the kinetics of water uptake (WU) by the hydrogel after freeze dried. The WU at higher cellulose content is less than the WU at lower cellulose content. The graph shows that the rate of WU is faster at the first 10 min and increase gradually until 80 min. Above 80 min of exposure, the increasing of WU has reached the equilibrium point in which the hydrogels has absorbed maximum of water. Increase the time after the saturation process will not increase the percentage of WU.

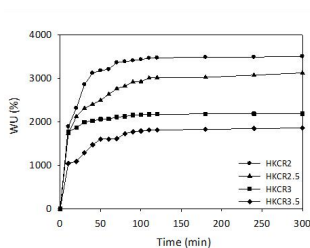


Figure 2 Rate of water uptake of cellulose hydrogel (a) HKCR2, (b) HKCR2.5, (c) HKCR3 and (d) HKCR3.5

Production of Cellulose Membrane

Figure 3 shows the morphology of the top side (contacting the coagulant) of the membranes casted on glass plate at different % of PVA. It is observed that the porosity of the membrane's surface increased with increasing of PVA content (Sawatari & Kondo 1999).

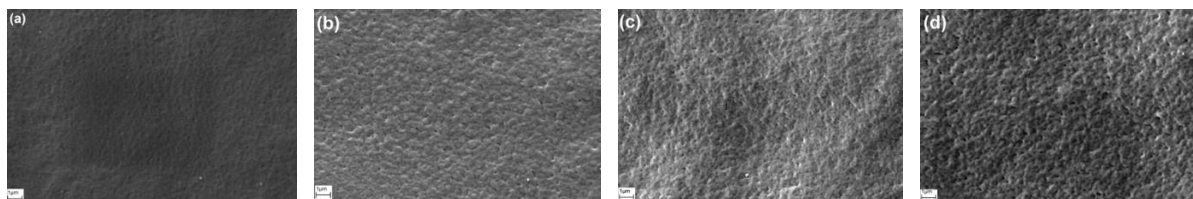


Figure 3 SEM images of the top side of membranes having CS/PVA in ratio (a) PVA0, (b) PVA1, (c) PVA5, and (d) PVA10

The scotch tape test is employed for estimating the adhesion strength of the ink on membranes. Figure 4(a) shows the printed membrane of PVA0 and PVA10; the ink on both printed membranes was removed using the tape test method. As can be seen in Figure 4(b) and 4(d), the ink was easier be removed from PVA10. This may due to the pore size of PVA10, which is larger than that of PVA0. The pore size will affect the ink detachment

because larger pore size makes the ink detachment easier when contact with water.

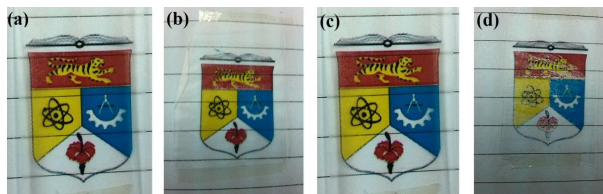
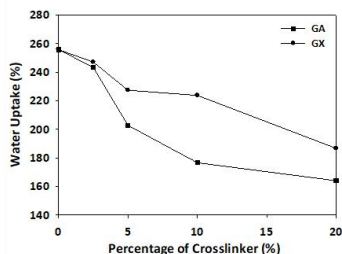
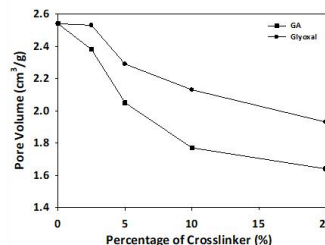


Figure 4 Photograph of (a) printed PVA0 membrane, (b) ink detached from PVA0, (c) printed PVA10 membrane, and (d) ink detached from PVA10

Figure 5(a) shows the water uptake (WU) of the membranes against percentage of crosslinker for both GA and glyoxal crosslinked cellulose membranes. It shows that as percentage of crosslinker increased, the value of WU has decreased. Cellulose membrane without crosslinker (DI) has the highest value of WU which is 256 % and reduced by 27 % and 26 % for both GA and glyoxal respectively at 20 % crosslinker. Figure 5(b) shows the pore volume (V_p) of cellulose membrane without crosslinker, GA crosslinked cellulose membrane and glyoxal crosslinked cellulose membranes at different crosslinker percentages. The V_p of DI membrane is $2.54 \text{ cm}^3\text{g}^{-1}$ and the value has decreased to 1.64 and $1.93 \text{ cm}^3\text{g}^{-1}$ which is decreased for both GA20 and GLO20 respectively. These results correspond to the water uptake where crosslinking process decreased both V_p and WU. This is due to the movement of molecular chain has been restricted by the crosslinking process (Li et al. 2014).



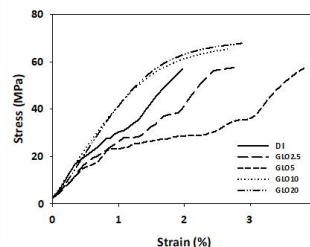
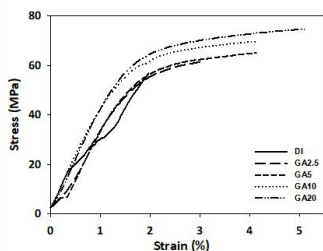
(a)



(b)

Figure 5 (a) Water uptake and (b) pore volume of cellulose membranes crosslinked with GA and glyoxal against percentage of crosslinker

Figure 6(a) and (b) show the stress versus strain curves of materials tested. As can be seen from the test, the higher the crosslinker content the higher the strength of the membranes. DI membrane possessed the lowest tensile strength which is 56 MPa. However, for glyoxal and GA crosslinked cellulose membranes, both show increment in tensile strength with increasing the crosslinker percentage up to 20 %. This has resulted in the increase in tensile strength up to 68 MPa and 75 MPa for both glyoxal and GA crosslinked cellulose membranes.



(a)

(b)

Figure 6 Stress-strain curve of cellulose membranes crosslinked with GA and glyoxal against percentage of crosslinker

Figure 7 shows the hysteresis loops of magnetic cellulose membrane (MCM) at different magnetite content i.e., 10 %, 20 % dan 30 % measured under VSM. MCM show that the membranes possessed ferromagnetic properties where there was a linear relationship between the magnetic properties and magnetite content. Therefore, increasing the magnetite content up to 30 %, saturation magnetization (M_s) becomes greater from 5.5 emu/g (MCM10) to 25.6 emu/g (MCM30). Figure 8 shows the XRD pattern of CM where three main diffraction patterns at $2\theta = 12.4^\circ$, 20.3° and 22.2° which corresponding to the cellulose II crystal at plane (1 $\bar{1}$ 0), (1 1 0) and (2 0 0), respectively. Meanwhile, the XRD pattern for Fe_3O_4 show six diffraction peaks at $2\theta = 30.19^\circ$, 35.58° , 42.91° , 53.46° , 57.24° and 62.63° respectively. These peaks correspond to the crystalline plane of Fe_3O_4 at (2 2 0), (3 1 1), (4 0 0), (4 2 2), (5 1 1) and (4 4 0). However, the crystallinity of the samples were decreased as increased the magnetite content from 71.4 % for CM to 44.7 % for MCM30.

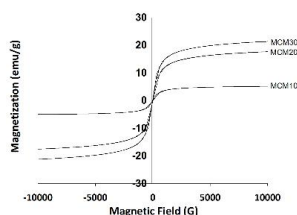


Figure 6 Hysteresis loops of magnetic cellulose membrane at different magnetite content

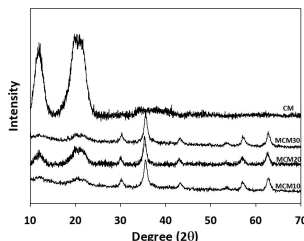


Figure 7 XRD patterns of cellulose membrane and magnetic cellulose membrane at different magnetite content

CONCLUSION

In summary, cellulose also can be extracted from kenaf core and others biomass plants. The extracted cellulose from biomass still can be a new natural biopolymer sources. This research used a low-cost production of regenerated cellulose materials and can be formed into biodegradable products. Research in regenerated cellulose materials using natural biopolymers can be extended into more applications such as membrane filtration for wastewater treatment, hydrophobic properties for water resistant products, coating and etc.

REFERENCES

- Chang, C., Zhang, L., Zhou, J., Zhang, L., & Kennedy, J.F. 2010b. Structure and properties of hydrogels prepared from cellulose in NaOH/urea aqueous solutions. *Carbohydrate. Polymers* 82: 122-127.
- Li, W., Wu, Y., Liang, W., Li, B. & Liu, S. 2014. Reduction of the water wettability of cellulose membrane through controlled heterogeneous modification. *Applied Materials and Interfaces* 6: 5726-5734.
- Mohd Edeerozey, A.M., Md Akil, H., Azhar, A.B. & Zainal Ariffin, M.I. 2007. Chemical modification of kenaf fibers. *Materials Letters* 61: 2023–2025.
- Sawatari, C. & Kondo, T. 1999. Interchain hydrogen bonds in blend films of poly(vinyl alcohol) and its derivatives with poly(ethylene oxide). *Macromolecules* 32: 1949-1955.
- Zhang, S., Li, F.X., Yu, J.Y. & Hsieh, Y.L. 2010a. Dissolution behaviour and solubility of cellulose in NaOH complex solution. *Carbohydrate Polymers* 81: 668–674.

CLASSIFICATION OF CANCER GENE SUBTYPES FROM CLUSTERING OF GENE EXPRESSION DATA

Logenthiran Machap¹, Afnizanfaizal Abdullah¹, Zuraini Ali Shah²

¹Synthetic Biology Research Group, School of Computing, Faculty of Engineering, Universiti Teknologi Malaysia

²Department of Software Engineering, School of Computing, Faculty of Engineering, Universiti Teknologi Malaysia

Abstract: Typically, microarray gene expression data obscure imperative information which is necessary for the understanding of molecular biology processes that occurs in a specific organism with respect to its environment. Uncovering gene expression data's invisible patterns will lead to a remarkable desire to enhance the interpretation of functional genomics. Biological networks intricacy and the presence of huge amount of genes raise the difficulties of understanding of the high dimension data, which resides lots of measurements. Thus, clustering techniques which are crucial in the data mining process are used as the first step to address this challenge to discover logical structures and predict significant patterns in the hidden data. These patterns may offer shreds of evidence about the biological process related to different physiological conditions. On deep, this paper focuses on the co-clustering algorithm to cluster genes and conditions simultaneously to obtain co-clusters further utilised for classification. The method called an improved network assisted co-clustering for the identification of cancer subtypes (iNCIS). Fundamentally, it integrates gene network information with gene expression to achieve biologically significant clusters. The classes obtained from clusters were used in the classification of genes to improve accuracy. This method applied to breast cancer and glioblastoma multiforme datasets. The discovered structures disclosed strong biological significance associations between functional annotations of genes with related conditions.

Keywords: *microarray, gene expression, clustering, classification*

INTRODUCTION

For decades, microarray technology has arisen as an effective technique to measure the expression levels of thousands of genes with various conditions. Molecular biologists have a key interest to detect genes expression levels which change in different experimental conditions where it is significant to understand gene regulation, gene function, cellular processes, gene subtypes and many more. However, for most of the available microarray datasets, the number of samples is small compared to thousands of genes (Yang and Naiman, 2014). It is essential to reduce the data for gene expression analysis which is necessary for advanced analysis such as clustering and classification (Liu *et al.*, 2008; Liu *et al.*, 2017).

OBJECTIVES

To propose classification of gene subtypes generated from unsupervised learning of an improved co-clustering algorithm

LITERATURE REVIEW

Conversely, most of the traditional clustering techniques have failed to identify co-regulated and co-expressed gene subsets under different experimental conditions. Therefore, co-clustering was replaced with traditional clustering to uncover local coherent patterns which reveal better biological certainty by simultaneously clustering the genes and samples. Co-clustering was applied different domain, such text mining (Lewis *et al.*, 2004), search in databases (Agrawal *et al.*, 1999), and target marketing (Wang *et al.*, 2002). While Cheng and Church (2000) are applied co-clustering also called ad bi-clustering techniques for gene expression data specifically

Consequently, unsupervised learning by clustering possible to use as a pre-processing step for supervised learning known as classification. Categorizing the genes into their respective class as normal or a tumour accurately will be done using the classifier. Examples of classifiers are support vector machine (SVM), neural network (NN), k-nearest neighbour (kNN) and classification tree (Lin and Chen, 2012).

METHODOLOGY

This paper, particularly presents our second objective which is the classification of cancer subtypes identified from the first objective where iNCIS adopted with support vector machine (SVM). Principally, clustering is unsupervised learning which is divided into two: soft and hard clustering. In hard clustering, variable from dataset fits precisely one cluster while in a soft clustering variable assigned to all the clusters with different probabilities or weights (Panda *et al.*, 2013). Through the improvement in the co-clustering technique provides the flexibility and options to generate different gene subtypes with better accuracy beside adapt to the classifier to obtain optimal classification accuracy of cancer gene identification. Figure 1 shows the general process of the proposed classification objective.

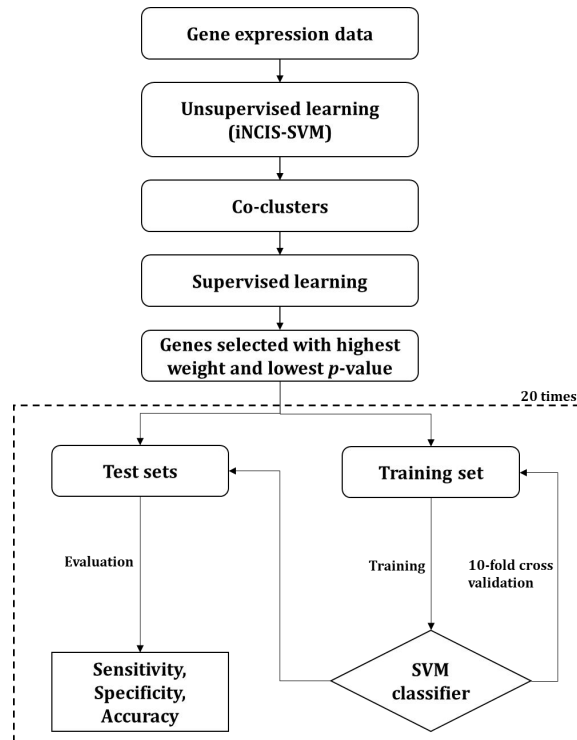


Fig. 1: The process of proposed classification after clustering

FINDINGS

For our analysis, we can conclude that the suitable range or amount of significant genes was 100, where both datasets have shown better or higher accuracy in this selected number of genes. Although the accuracy difference was not irregular, the selected numbers of gene were either too less or too many compared to other selections. However, other selection variance of genes can be used by other researchers for consequent analysis besides filtering of genes for huge datasets. In between, the selection of genes can be varied according to requirements for example, gene network analysis, gene ontology for gene functional annotation many more.

Table 1: Prediction accuracy for various gene selections range and accuracy comparison

Genes	Method	iNCIS+SVM		NCIS+SVM	
		BRCA	GBM	BRCA	GBM
35		0.936	0.928	0.901	0.913
50		0.945	0.931	0.932	0.903
100		0.952	0.941	0.902	0.890
200		0.931	0.892	0.932	0.900

From the comparison, (Figure 2) can conclude that overall our method has raised the classification accuracy for both datasets used. The average improvement from previous work with our results is a 1.03% increase in accuracy for breast cancer dataset and 1.02% accuracy increment for the glioblastoma multiforme dataset. This improvement was achieved because the improvement made in the clustering process help us to select more significant genes compared to previous research.

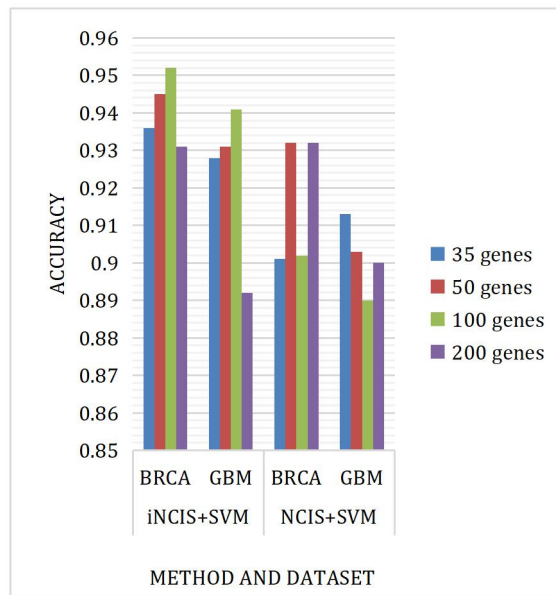


Fig. 2: Prediction accuracy comparison

CONCLUSION

Gene expression classification of patient samples has been focused on cancer diagnosis and prognosis. To deal with the high dimensionality of data and low classification accuracy our method outperforms the previous research methods of identifying biologically significant genes. These genes justification analysis carried out further in terms of the functions of genes and pathway analysis.

REFERENCES

- Agrawal, R., Gehrke, J. E., Gunopulos, D., and Raghavan, P. (1999). Automatic subspace clustering of high dimensional data for data mining applications: Google Patents.
- Cheng, Y., and Church, G. M. (2000). *Biclustering of Expression Data*. Paper presented at the Proceedings of the Eighth International Conference on Intelligent Systems for Molecular Biology.
- Lewis, D. D., Yang, Y., Rose, T. G., and Li, F. (2004). Rcv1: A new benchmark collection for text categorization research. *Journal of machine learning research*, 5(Apr), 361-397.
- Lin, W.-J., and Chen, J. J. (2012). Class-imbalanced classifiers for high-dimensional data. *Briefings in bioinformatics*, 14(1), 13-26.
- Liu, W., Yuan, K., and Ye, D. (2008). Reducing microarray data via nonnegative matrix factorization for visualization and clustering analysis. *Journal of Biomedical Informatics*, 41(4), 602-606.
- Liu, Y., Wu, S., Liu, Z., and Chao, H. (2017). A fuzzy co-clustering algorithm for biomedical data. *PLOS ONE*, 12(4), e0176536.
- Panda, B., Sahoo, S., and Patnaik, S. K. (2013). A comparative study of hard and soft clustering using swarm optimization. *International Journal of Scientific & Engineering Research*, 4(10), 785-790.
- Wang, H., Wang, W., Yang, J., and Yu, P. S. (2002). *Clustering by pattern similarity in large data sets*. Paper presented at the Proceedings of the 2002 ACM SIGMOD international conference on Management of data, 394-405.
- Yang, S., and Naiman, D. Q. (2014). Multiclass cancer classification based on gene expression comparison. *Statistical applications in genetics and molecular biology*, 13(4), 477-496.

The Synergistic Antibacterial Effects of *Cinnamomum verum* and *Cymbopogon citrates* on Urinary Tract Infections causing pathogens *Escherichia coli* and *Pseudomonas aeruginosa*

Fional Lawing¹, Noor Faradilla Abdullah¹, Che Wan Imanina Che Wan Takwa¹

¹Faculty of Health Sciences, aSIA Metropolitan University Selangor, Malaysia

Abstract: *Escherichia coli* (E.coli) and *Pseudomonas aeruginosa* (P. aeruginosa) have been one of the few main pathogens that lead to urinary tract infection. The study was conducted because there have been an increase in antibiotic resistance pattern in the world. Ethanol and aqueous extract of medicinal plant, cinnamon, *Cinnamomum verum* and lemongrass, *Cymbopogon citrates* were prepared to test its synergistic antibacterial effect against . The test was then preceded with the Minimum Inhibitory Concentration (MIC) using the 96 well microtitreplate. The Minimum Bacterial Concentration (MBC) were then attained after the the MIC result were observed. The MIC of E.coli was at 6.25 µg/mL for the synergy ethanolic extract between *Cinnamomum verum* and *Cymbopogon citratus*. The aqueous extract did not visualize any growth inhibition on the bacteria E.coli. Both ethanolic and aqueous extract also had no inhibitory effect on the P. aeruginosa. The synergistic extract of *Cinnamomum verum* and *Cymbopogon citratus* was effective against E. coli. Therefore, it was concluded that the effect of the extract was effective on E. coli and it was almost as effective as the antibiotics that were usually prescribed for the treatment of urinary tract infections.

Key words: Synergy, *Cinnamomum verum*, *Cymbopogon citratus*, *Escherichia coli*, *Pseudomonas aeruginosa*.

INTRODUCTION

Antibiotic treatment has been widely used for the treatment of urinary tract infection, this has also contributed to the rise of antibiotic resistance in the population. From 2000 to 2010, the antimicrobial resistance of urinary tract pathogen, *Escherichia coli* towards the antibiotic ciprofloxacin and trimethoprim and sulfamethoxazole have increased rapidly. Cinnamon is one of the most well known common spices that can be found all over the world. It has also been used both as cooking material and medicine over thousands of years. Cinnamon comes from the family of *Lauracea*. The cinnamon is derived from the inner bark of trees from the genus *Cinnamomum*. The other plant that was used in this synergistic antibacterial study was lemongrass. The plant is scientifically known as *Cymbopogon citratus* (*C.citratus*). One of the recent studies have stated that the ethanolic extracts of the leaves of lemongrass showed potential antibacterial property against *Staphylococcus aureus*.

OBJECTIVE

the main aim of this study was to investigate the synergistic antibacterial effect of cinnamon, *Cinnamomum verum* and lemongrass, *Cymbopogon citratus* against *Escherichia coli* and *Pseudomonas aeruginosa*.

METHODOLOGY

<p>Plant Extraction</p>	<ul style="list-style-type: none"> • Cut the plant into small pieces. • soaked briefly with distilled water before blotting the excess water with tissue paper. • placed in a clean steel tray and were set in the hot air oven at 40°C. • left to dry in the oven. • the plants had to be finely grinded using a dry blender to obtain the powdered formed. • about 200g of fine powder of both plants were weighed and were soaked in 600ml of 95% of ethanol and water. • soaked for 3 days. • The aqueous extract were placed in the hot air oven at 40°C while the ethanolic extracts were
--------------------------------	---

	<p>be concentrated using the rotary evaporator also at 40°C.</p> <ul style="list-style-type: none"> Finally, the extracts were chilled in the refrigerator until used at 4°C.
<p>Bacterial Strains (Inoculum Preparation)</p>	<ul style="list-style-type: none"> Cultured the pure culture-24 hours at 37° C. stored at 4° C to maintain its growth. The inoculums were prepared by growing the sub culturing the bacteria that had been made in Mueller Hinton broth at the temperature of 37° C, overnight.
<p>Antibiotic Susceptibility Test</p>	<ul style="list-style-type: none"> using the disk diffusion method (Kirby Baur test). bacteria inoculum was prepared by inoculating a single colony of the bacteria <i>E. coli</i> and <i>P. aeruginosa</i> into the Mueller Hinton broth (incubated at 37°C overnight). the paper disk which contained single concentration of each antimicrobial agent will be set on the surface of the agar that has been inoculated with the bacteria. blank disc that had been soaked in the extract of the <i>C. verum</i> and <i>C. citratus</i> were also placed on the agar for testing. Three different concentration of tested plant extract were prepared (20 mg/mL, 50 mg/mL and 100 mg/mL). For <i>E. coli</i>, the positive control that was used for the experiment was ciprofloxacin. As for <i>P. aeruginosa</i>, the positive control was gentamicin). The negative control used for both organism was distilled water for aqueous extract, 10% DMSO for ethanolic extract. The extract of the cinnamon and lemongrass antibacterial effect would be compared with the commonly used antibiotic. the agar plate was left to be incubated overnight at 37°C and measurement of inhibition zone was taken the following day.

FINDINGS

As stated by Ochei et al. in the book of Medical Laboratory Science, Theory and Practice year 2000, there are a few factors that can affect this antimicrobial susceptibility test. The first is the depth of the medium. The depth of the media that is being used may affect the result as it can interact and disturb the concentration gradient of the diffusing antibacterial or antimicrobial agent. Thicker agar medium will give out smaller zone of inhibition while thinner agar medium will produce a larger zone. In order to standardize, it is advisable to pour 25 ml of medium in agar plate which will produce an agar with the depth of 4mm. Next factor that can interfere with the test is the atmosphere of the incubator. The incubation is recommended to be carried out in incubator with ambient air. If the incubation is carried out, for an example in a carbon dioxide incubator, it may result in decrease pH of the agar, thus affecting the action of some drugs.

CONCLUSION

The synergistic ethanolic extract of *Cinnamomum verum* and *Cymbopogon citratus* was effective against one of the bacteria which were *E. coli*. The result that were obtained had also shown that effect of the extracts were almost as effective as the antibiotics that were usually prescribed for the treatment of urinary tract infections. To ensure the safety of the extract, the extract can also be tested against the normal flora of the urinary tract. Toxicity test of the extract can also be done. The extract can also be tested on extended spectrum beta lactamase (ESBL) bacteria, in order to know more about its effect on Gram negative bacteria.

SELECTIVE REFERENCES

1. Al-Badr, A., & Al-Shaikh, G. (2013). Recurrent urinary tract infections management in women: A review. Sultan Qaboos University Medical Journal, 13(3), 359–367.

Nabavi, S. F., Di Lorenzo, A., Izadi, M., Sobarzo-Sánchez, E., Daglia, M., & Nabavi, S. M. (2015). Antibacterial effects of cinnamon: From farm to food, cosmetic and pharmaceutical industries. *Nutrients*, 7(9), 7729–7748. <https://doi.org/10.3390/nu7095359>

Densification behavior and mechanical properties of Cerium Oxide and Manganese Oxide-doped Ytria Tetragonal Zirconia Polycrystals Ceramics for Dental Applications.G. Sankar¹, S. Meenaloshini², R. Dinesh³¹Department of Mechanical Engineering, Universiti Tenaga Nasional, Kajang, 43000, Malaysia,

sankarsaisanjay@gmail.com

²Department of Mechanical Engineering, Universiti Tenaga Nasional, Kajang, 43000, Malaysia,

Meenaloshini@uniten.edu.my

³Department of Mechanical Engineering, Universiti Tenaga Nasional, Kajang, 43000, Malaysia,

dineshragurajan@gmail.com

The densification behaviour, mechanical properties, and microstructure of high-purity CeO₂ and MnO₂-doped Y-TZP with different weight percentage varied from 0.5 to 1.5wt% were investigated. The samples were pressed uniaxially at 200 MPa into rectangular bars and discs and pressureless-sintered at temperatures ranging between 1250°C and 1450°C for 1h holding time while the microstructure was characterized with a scanning electron microscope (SEM). It was found that the mechanical properties of Y-TZP were dependent on the dopant amount and sintering temperature. The mechanical properties in terms of bulk density, Young's modulus, Vickers hardness, and fracture toughness were also measured. The results indicate that the addition of dopants accelerated the densification parameters and reinforced and toughened the obtained bodies. The best values for the mechanical properties of the CeO₂ and MnO₂-doped Y-TZP ceramics were 5.67 Mgm-3 and 8.46 GPa for density and Vickers hardness, respectively, which are higher than those of the undoped samples. The best flexural strength and Young modulus obtained from the experiment are ~900 MPa and 210 GPa respectively. These results were with the addition of 0.5wt% MnO₂ and 0.5wt% CeO₂ sintered at 1350°C.

Keywords: CeO₂, MnO₂, Mechanical Properties, Microstructure

Introduction

Zirconia holds a unique place amongst oxide ceramics because of its excellent mechanical properties. Zirconia that contains ceramics are materials of imparting toughness which is known as transformation toughening, while maintaining strength and chemical inertness, and of exhibiting new functions such as shape memory effect by manipulating new microstructure. Ytria-stabilised tetragonal zirconia polycrystalline ceramics (Y-TZP) are becoming popular engineering materials due to their excellent mechanical properties, studied and used in many engineering applications, such as engine parts, valves, cutting tools, and moulds, due to their good fracture toughness, high strength, elastic modulus, and wear resistance (R. Stevens, 1986, L. Gakovic, 2007, P. Christel et al., 1989).

Objectives

The research objective is to find the most optimum MnO₂ and CeO₂ dopant content into Y-TZP and the best sintering temperature for 1 hour holding time to maintain the best mechanical properties results i.e bulk density, Vickers hardness, Youngs modulus and flexural strength.

Literature Review

The stabilizing effect of yttria makes it possible for Y-TZP ceramic to be processed in the metastable tetragonal (t) structure. This is essential since the retention of the (t) phase at ambient temperature allows it to transform to the monoclinic (m) structure under external applied stress (P.M Kelly, 2002, K. Matsui et al., 2008). However, in spite of the many favorable characteristics such as high strength, high toughness and good wear properties, Y-TZP ceramics display an unfavorable low temperature ageing phenomenon especially in humid atmosphere (water and steam) at

temperatures ranging from 20°C to 500°C, a phenomenon widely known as low temperature degradation (LTD) or hydrothermal ageing (Claudia A.M.V et al., 2011, Shukla, 2005). The degradation which occurs is normally accompanied by mechanical property deterioration attributed to the ageing-induced tetragonal (t) to monoclinic (m) phase transformation.

Since then, experiments have been conducted with Y-TZP in an attempt to understand the basic micro mechanisms of the ageing-induced (t)-(m) phase transformation and to suppress the LTD phenomenon (P. Kohorst et al., 2012, L. Borchers et al., 2010, F. Egilmez et al., 2014, J. Valle et al., 2013, H.P Papanagiotu et al., 2006, J. Chevalier, 2006, T. Kosma, 2008, M. Cattani-Lorente et al., 2014, N. Masahiro et al., 2014). Based on research findings, the addition of ceramic oxides (MgO, Al₂O₃, ZnO, CaO, and CeO₂) help overcome if not prevent the low temperature degradation occurrence in Y-TZP ceramics (X. Guo 2003, X. Guo., 2004, V. Lughi, 2010, J.R. Kelly, 2008, Hallmann et al., 2012). CeO₂ is generally used to stabilize the tetragonal phase of zirconia and is also known to increase the sintering of glass ceramics and strength and thermal stability. This work present effect of different parameter on the surface morphology, particle distribution and size of ZnO nanoparticles prepared using LP-PLA technique.

Methodology

The base powder, a co-precipitated sprayed dried 3mol% yttria-zirconia (Y-TZP) was manufactured and supplied by Kyoritsu Japan. Varying amounts of high purity CeO₂ and MnO₂ (undoped, 0.5, 1.0 and 1.5wt%, Sigma Aldrich) doped Y-TZP powders were prepared by a wet colloidal method, using zirconia balls as the milling media and ethanol as the mixing medium. The slurry was oven dried and sieved to obtain soft, ready-to-press powder.

Disc (20 mm diameter) and rectangular bar samples were compacted at 0.3 MPa and isostatically pressed at 200 MPa. Consolidation of the particles by pressureless sintering was performed in air using a rapid heating furnace (ModuTemp, Australia), at various temperatures ranging from 1250°C to 1450°C, maintained at the holding temperature for 1h before cooling to room temperature. The sintered samples were ground on one face by SiC papers of 120, 240, 600, 800 and 1200 grades successively, followed by polishing with 6 μ diamond paste to produce an optical reflective surface. The bulk density of the sintered samples was measured based on Archimedes' principle using an electronic balance retrofitted with a density determination kit (Mettler Toledo, Switzerland).

The Young's modulus (E) by sonic resonance was determined for rectangular samples using a commercial testing instrument (GrindoSonic: MK5 "Industrial", Belgium). The instrument permits determination of the resonant frequency of a sample by monitoring and evaluating the vibrational harmonics of the sample by a transducer; the vibrations are physically induced in the sample by tapping. The modulus of elasticity or Young's modulus was calculated using the experimentally determined resonant frequency (ASTM, 1998). Fracture toughness and Vickers hardness measurements (Future Tech., Japan) were made on polished samples using the Vickers indentation method. The indentation load was kept constant at 98.1 N and a loading time of 10 s was employed. The values of K_{1c} were computed using the equation derived by Niihara et al. (Niihara K et al.,1982). Average values were taken from five measurements. The microstructure of the samples was examined by JSM-6310 scanning electron microscopy (SEM).

Findings

The best dopant content into Y-TZP is 0.5wt% CeO₂ and 0.5wt% MnO₂ at a sintering temperature of 1350°C. The mechanical properties results obtained were good, the bulk density is 5.67 g/cm³, approximately 94% of the theoretical density of Y-TZP. The other mechanical properties, Vickers hardness is 8.46 GPa, Young's modulus is of 200GPa and flexural strength is ~900 MPa.

Conclusion

The results from this research show that the mechanical properties of the compositions have been enhanced by the addition of 0.5wt% CeO₂ and 0.5wt% MnO₂ with Y-TZP. The value of density achieved was about 5.67 g/cm³, approximately 94% of the theoretical density of Y-TZP. The other mechanical properties (i.e. hardness and flexural

strength) of the material also experienced significant increase. In addition to that, the 0.5wt% CeO₂ and 0.5wt% MnO₂ composite displayed higher Young's modulus of 200GPa. Sintering above 1450°C has shown degeneration in the composite's physical and mechanical properties. Sintering at higher temperatures (>1350°C) had affected the mechanical properties of the composite, due to bigger grain size obtained at higher temperature. The hydrothermal degradation test to be conducted.

Main References

Bao L., Liu J., Shi F., Jiang Y., Liu G.: Preparation and characterization of TiO₂ and Si-doped octacalcium phosphate composite coatings on zirconia ceramics (Y-TZP) for dental implant applications. *Applied Surface Science*, 290, 48-52 (2014)

M. Cattani-Lorente, S. S. Scherrer, S. Durual et al., "Effect of different surface treatments on the hydrothermal degradation of a 3Y-TZP ceramic for dental implants," *Dental Materials*, 2014

Cláudia A.M.V., Luis G.D.A.G, Márcio C.F., Federica B.: Application of Zirconia in Dentistry: Biological, Mechanical and Optical Considerations, *Advances in Ceramics -Electric and Magnetic Ceramics, Bioceramics, Ceramics and Environment*, 397-420 (2011)

Yin Z., Yan S., Wenda L., Shengxiang J., Weijing C., Zhenning W., Kun W.: Effect of MgO doping on properties of low zirconium content Ce-TZP/Al₂O₃ as a joint replacement material. *Ceramics International*, 43, 2, 2807–2814 (2017)

J. Valle, A. Mestra, F. G. Marro, and M. Anglada, "Mechanical properties and resistance to low temperature degradation of surface nitrided 3Y-TZP," *Journal of the European Ceramic Society*, vol.33,no.15-16,pp.3145–3155,2013

Effect of CeO₂ and MnO₂ on the Microstructure, Degradability and Mechanical Properties of Zirconia

D. Ragurajan^a, M. Satgunam^a, U. Sankar^a, M. Golieskardi^a

¹Department of Mechanical Engineering, Universiti Tenaga Nasional, Kajang, 43000, Malaysia, dineshragurajan@gmail.com

²Department of Mechanical Engineering, Universiti Tenaga Nasional, Kajang, 43000, Malaysia, Meenaloshini@uniten.edu.my

³Department of Mechanical Engineering, Universiti Tenaga Nasional, Kajang, 43000, Malaysia, sankarsaisanjay@gmail.com

⁴Department of Mechanical Engineering, Universiti Tenaga Nasional, Kajang, 43000, Malaysia, mohsen_golieskardi@yahoo.com

The influence of small additions of CeO₂ and MnO₂ (up to 1 wt%) on the sintering behaviour of yttria-stabilized zirconia sintered from 1250°C to 1450°C was investigated. The results revealed that relative densities above 97.5% of theoretical (i.e. > 6.01 Mgm⁻³) could be obtained in Y-TZPs sintered at low temperatures, 1250°C and 1300°C, with the additions of 0.3 wt% MnO₂. In comparison to the undoped samples, the additions of up to 1 wt% CeO₂ and MnO₂ and for sintering up to 1350°C was found to be beneficial in enhancing the Vickers hardness of the ceramic. The highest hardness value of approximately 9.4GPa was achieved for the 0.2wt% of CeO₂ and 0.8wt% of MnO₂ composition for samples sintered at 1250°C. It was evident that the addition of CeO₂ and MnO₂ to Y-TZP yielded an increase in flexural strength, whereby 0.2wt% CeO₂/0.8wt% MnO₂ samples recorded highest value of strength; increasing from ~550MPa at 1250°C to ~930MPa at 1350°C. It was found that the 0.2wt% CeO₂ /0.8wt% MnO₂ samples achieved the highest E value of 220GPa at 1350°C, slightly higher than theoretical value of the Young's modulus of pure Y-TZP material (200GPa). The SEM analysis revealed that 0.2wt% CeO₂/0.8wt% MnO₂ samples exhibited an average grain size value of approximately 464.92nm while the 0.5wt% CeO₂/0.5wt% MnO₂ recorded an average grain size value of 533.72nm. Consistently, it was found that the 0.2wt% CeO₂/ 0.8wt% MnO₂ -doped 3Y-TZPs sample exhibited the best ageing resistance with 36% transformation after being subjected to ageing conditions for 10 hours.

Keywords: Mechanical Properties, CeO₂, MnO₂, Microstructure, Degradation

Introduction

Yttria stabilized tetragonal zirconia polycrystals or subsequently known as Y-TZP, is an advanced ceramic, engineered to take full advantage of the transformation toughening effect [Bikramjit et.al (2004), Aksel et.al. (2003)]. This ceramic, when fired, consists of a single phase tetragonal structure of fine grains (< 0.5 μm) which makes it ideal for many structural applications due to its excellent strength, high toughness and good wear resistance [Anthony(2016), Claussen (1985), Fukahori et.al. (2016), Seidensticker (1994)].

Objectives

The aim of the present work was to study the influence of adding small amounts of Cerium oxide and manganese oxide (up to 1 wt %) on the on densification and mechanical properties of yttria-stabilized zirconia..

Literature Review

Generally, Y-TZP is used in application such as biomedical implant, sandblasting nozzles, sharp edges of scissors and knives, and metal cutting tools [Piconi et.al. (1999), McDonald (2007)].

However, in spite of the many favorable characteristics such as high strength, high toughness and good wear properties, Y-TZP ceramics display an unfavorable low temperature ageing phenomenon especially in humid atmosphere (water and steam) at temperatures ranging from 20°C to 500°C, a phenomenon widely known as low temperature degradation (LTD) or hydrothermal ageing [Claudia et.al. (2011), Shukla et.al. (2005), Lange et.al. (1982)]. The degradation which occurs is normally accompanied by mechanical property deterioration attributed to the ageing-induced tetragonal (t) to monoclinic (m) phase transformation.

A frequent method that has been used to suppress ageing is the use of appropriate sintering additives or dopants in Y-TZP. Small or even minute amounts of additives can promote densification and substantially control the microstructure as well as to enhance the mechanical properties of the sintered body. The beneficial effect of transition metal oxide additions in suppressing the ageing-induced (t) to (m) phase transformation has been reported by several researchers [Kimura et.al. (1989)]. In particular, the addition of MnO₂ and CuO to Y-TZP has been observed to result in enhanced sinterability, finer grain sizes and higher fracture toughness. These effects were reported by [Kwa et.al. (2015), Ramesh et.al. (1999), Lawson et.al. (1995), Kanellopoulos et.al. (2002)].

It has been reported that improved Y-TZPs with optimized mechanical properties and ageing resistant could be obtained by the addition of more than one stabilizer to zirconia [Xu et.al. (2004)]. It was found that the addition of CeO₂ to Y-TZP could prevent ageing, while retaining relatively high fracture toughness of 7–9MPam^{1/2}.

Methodology

The base powder, a co-precipitated sprayed dried 3 mol% yttria-zirconia (Y-TZP) was manufactured and supplied by Kyoritsu Japan. Varying amounts of high purity CeO₂ and MnO₂ (0.05, 0.1, 0.3, 0.5 and 1 wt%, Sigma Aldrich) doped Y-TZP powders were prepared by a wet colloidal method, using zirconia balls as the milling media and ethanol as the mixing medium. The slurry was oven dried and sieved to obtain soft, ready-to-press powder. Disc (20 mm diameter) and rectangular bar samples were compacted at 0.3 MPa and isostatically pressed at 200 MPa. Consolidation of the particles by pressureless sintering was performed in air using a rapid heating furnace (ModuTemp, Australia), at various temperatures ranging from 1250°C to 1450°C, maintained at the soak temperature for 2 h before cooling to room temperature. Both weight percentages and sintering parameters were determined and finalized by preliminary tests results. The sintered samples were ground on one face by SiC papers of 120, 240, 600, 800 and 1200 grades successively, followed by polishing with 6 μ diamond paste to produce an optical reflective surface. The bulk density of the sintered samples was measured based on Archimedes' principle using an electronic balance retrofitted with a density determination kit (Mettler Toledo, Switzerland).

The Young's modulus (E) by sonic resonance was determined for rectangular samples using a commercial testing instrument (GrindoSonic: MK5 "Industrial", Belgium). The instrument permits determination of the resonant frequency of a sample by monitoring and evaluating the vibrational harmonics of the sample by a transducer; the vibrations are physically induced in the sample by tapping. The modulus of elasticity or Young's modulus was calculated using the experimentally determined resonant frequency [ASTM Standard E1876-97 (1989)]. Fracture toughness and Vickers hardness measurements (Future Tech., Japan) were made on polished samples using the Vickers indentation method. The indentation load was kept constant at 98.1 N and a loading time of 10 s was employed. These tests are in accordance to [ASTM E384-99(1999)] and [ISO 14705(2000)]. The values of K_{Ic} were computed using the equation derived by [Niihara et.al. (1982)]. Average values were taken from five measurements.

Findings

The best additive content into Y-TZP is 0.2wt% CeO₂ and 0.8wt% TCP at a sintering temperature ≤1350°C. The mechanical properties results obtained showed that the bulk density was slightly enhanced to 6.04 g/cm³, approximately 98% of the theoretical density value, 9.4GPa for the Vickers hardness, a flexural strength of 930MPa and Young's Modulus of 220GPa respectively.

Conclusion

The results from this research show that the mechanical properties were improved by addition of 0.2 wt% CeO₂ and 0.8 wt% MnO₂ with Y-TZP. This composition increased the density of Y-TZP. The value of density achieved was about 6.04 g/cm³, approximately 98% of the theoretical density of Y-TZP. The mechanical properties (i.e. hardness and strength) of the material were significantly increased as well. Besides that, the 0.2 wt% CeO₂ and 0.8 wt% MnO₂ composite displayed higher elasticity of 211 GPa compared to pure Y-TZP with a theoretical value of 200 GPa. Sintering over 1450 °C is expected to degenerate the composite's physical and mechanical properties. Sintering at higher temperatures (>1350 °C) would affect the properties of the composite, due to a bigger grain size obtained at high temperature.

Main References

- B. Bikramjit, J. Vleugels and O.B. Vander (2004). Microstructure-Toughness-Wear Relationship of Tetragonal Zirconia Ceramics, *J. Eur. Ceram. Soc.*, 24: 2031-2040.
- C. Aksel (2003). Mechanical Properties and Thermal Shock Behaviour of Alumina-Mullite-Zirconia and Alumina-Mullite Refractory Materials by Slip Casting, *Ceram. Int.*, 29: 311-316.
- A.M. Anthony (2016). Effect of sintering temperature on mechanical properties of magnesia partially stabilized zirconia refractory, *Ceram. Int.*, 42, 9: 10593–10598.
- N. Claussen (1985), Strengthening Strategies for ZrO₂-Toughened Ceramics at High Temperatures, *Mater. Sci. Eng.*, 71: 23-38.
- R. Fukahori, T. Nomura, C. Zhu, N. Sheng, N. Okinaka and T. Akiyama (2016). Thermal analysis of Al–Si alloys as high-temperature phase-change material and their corrosion properties with ceramic materials, *Appl. Energy*, 163: 1–8.
- J.R. Seidensticker and M.J. Mayo (1994). Superplasticity in 3Y-TZP Doped With Small Amounts of Copper Oxide, *Scr. Metall. Mater.*, 31: 1749-1754.
- C. Piconi and G. Maccauro (1999). Zirconia as a Ceramic Biomaterial, *Biomaterials*, 20: 1-25

LINEAR HYBRID CELLULAR AUTOMATA (LHCA) RULE 90/150 BASED S-BOX

Muhammad Fahim Roslan¹, Kamaruzzaman Seman², Azni Haslizan Ab Halim³, M
Norazizi Md Sayuti⁴

¹Fakulti Kejuruteraan dan Alam Bina, Universiti Sains Islam Malaysia

²Fakulti Kejuruteraan dan Alam Bina, Universiti Sains Islam Malaysia

³Fakulti Sains dan Teknologi, Universiti Sains Islam Malaysia

⁴Fakulti Kejuruteraan dan Alam Bina, Universiti Sains Islam Malaysia

Abstract: Most modern block cipher today comprises of single nonlinear element which is called as substitution box. It comes with various of size depending on the cipher input and the secret key. Various methods have been proposed in order to construct it. In this paper, a new construction method has been proposed that is based on linear hybrid cellular automata (LHCA) iteration. There are specific number of combinations of rule 150 and rule 90 of elementary cellular automata (ECA) with two states and three neighborhoods that generate maximum cycle sequence which usually adapted as pseudo random number generator. However, the sequence is actually the permutation of finite elements which is suitable for the S-Box construction. Within this paper context, we manipulate the sequence by varying the initial condition to produce about 8192 different S-Box with different security level from 32 different rule combination. The maximum nonlinearity that we could achieve is 108 with differential uniformity value of 8.

Keywords: Cryptography, Block Cipher, Cellular Automata, Primitive Polynomial

INTRODUCTION

A frequent discussed topic in block cipher is the construction and implementation of the substitution box (S-Box). The trend of most modern block cipher design only adapt one nonlinear component while the rest use linear transformation or permutation. It can be seen in the implementation of data encryption standard (DES), advanced encryption standard (AES), PRESENT and many others. Hence, it is important to select the best method of S-Box construction and implementation so that the cipher will have efficient operation time and optimum security level. Even though an S-Box acts as the main component of any block cipher, the operation is simply substitutes the input with the predefined value from the fixed table. Hence it also can be viewed as a mapping of the set of finite input to the set of finite output. Besides, its implementation method have also been widely discussed as the evolution of cryptanalysis methods have emerge rapidly. As in this paper, we proposed a method of construction with new implementation. The construction method is based on the linear hybrid cellular automata (LHCA) method. This method is based on the iteration of elementary cellular automata that have been described in detailed in Wolfram (2002).

In the next section, some preliminary concept regarding S-Box as vectorial Boolean function is discussed. Besides, as the same section, the preliminary definition of cellular automata is also presented. At section 3, some relevant studies related to cellular automata and its application in cryptography is presented. Section 4 continue with the methodology of the proposed construction methods together with complete pseudo code. The analysis in term of cryptography properties and the security of constructed S-Box is presented in section 5. The last section concludes the paper.

PRELIMENARIES CONCEPT

Vectorial Boolean Function

This section presents some fundamental aspects of vectorial Boolean function in the application of cryptography block cipher. An S-Box can be interpreted as vectorial Boolean function which received -binary input and generate -binary output. Let be a vector space of -variables with the cardinality of . Then an S-Box can be viewed as map where each and each can be assigned as . The map comprises of -single Boolean functions which can be defined as where . Most cryptography properties are evaluated based on these functions which also can be referred as coordinate function . In evaluating S-Box, several representations may be used such as truth table, polarity truth table and algebraic normal form. The truth table is simply the collection of all output of Boolean function with the input vector arranged in lexicographical order and has the dimension of . The polarity truth table on the other hand, is made up of the sign function expressed as which yield the output of and for the input of and 1 respectively. Despite the truth table, another representation, the algebraic normal form (ANF) represent the Boolean function in term of polynomial. In general, the ANF of any Boolean function with variables can be expressed as

$$g(x) = c_0 \oplus_{1 \leq i \leq n} c_i x_i \oplus_{1 \leq i < j \leq n} c_{ij} x_i x_j \oplus \dots \oplus c_{1\dots n} x_1 x_2 \dots x_n \quad \text{* MERGEFORMAT (1.1)}$$

where the coefficient having the value of either and . Each Boolean function of variables will have its own unique ANF. The longest term in ANF determine the algebraic degree of the Boolean function . The function is called affine function if the longest term equal to 1, while with the absence of constant term , the function is categorized as linear Boolean function.

Cryptography Properties

The cryptography properties are the set of tools that quantify the security of any given substitution box. It comprises of several quantity in which the most essential are the nonlinearity, differential uniformity, algebraic degree and balancedness. The nonlinearity is a measure of distance of any Boolean function to the set of all affine function , that is

$$N_g = \min_{a \in \mathbb{F}_2^n, b \in \mathbb{F}_2} \text{dist}(g, \ell_{a,b}) \quad \backslash^* \text{MERGEFORMAT (1.2)}$$

where ; denote the inner product and as a XOR Boolean operator. The distance mentioned in Eq.2 means the hamming distance. Higher value of is more favorable as it indicates greater distance to the set of all affine function. Frequently, the quantity is evaluated using the Walsh-Hadamard Transform (WHT) that utilize the sign function which can be expressed as

$$W_g(\omega) = \sum_{x \in \mathbb{F}_2^n} (-1)^{\langle x, \omega \rangle \oplus g(x)} \quad \backslash^* \text{MERGEFORMAT (1.3)}$$

The evaluation of the above equation on any S-Box is done on each coordinate function where the minimum one is taken as the value of nonlinearity .Differential uniformity is another quantity that defined the security of cryptography algorithm against differential analysis (Biham & Shamir, 1990). It analyzes the relationship between the difference in plaintext and its corresponding difference in ciphertext. This quantity is defined by the minimum entry of the differential distribution table denoted by parameter as follows,

$$\delta = \max_{a, b \in \mathbb{F}_2^n, a \neq 0} \left| \{x \in \mathbb{F}_2^n : S(x+a) + S(x) = b\} \right| \quad \backslash^* \text{MERGEFORMAT (1.4)}$$

This parameter only takes even value with the smallest value indicates better resistance against differential analysis. The algebraic degree of an S-Box is defined as the maximum algebraic degree of all coordinate functions . Higher algebraic degree is preferable in order to thwart higher-order differential attacks.

Cellular Automata

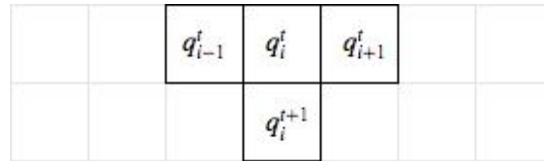
The cellular automata (CA) are parallel computation models which have been adapted in plenty of applications. In cryptography, CA is widely used as a part of pseudo-random number generator (PRNG) algorithm. It also have been adapted as nonlinear element in block cipher such as in Keccak (Bertoni et al., 2011). Basically, CA is characterized by the lattice cells of finite dimension which evolve in time synchronously according to the local rule and state of neighborhoods. The most basic CA was characterized briefly by Stephen Wolfram (Wolfram, 2002) known as elementary cellular automata (ECA) that is build up with one dimensional CA with three neighborhood and two states. Formally, it can be defined as follows,

$$C = (Q, r, f) \quad \backslash^* \text{MERGEFORMAT (1.5)}$$

where for and that represent the set of interconnected cells arranged in regular manner as can be seen in Fig.1. is the set of states for each cell and specified the size of neighborhood. ECA only have two states that is represented by binary variables 1 or 0. Each cell evolve in discrete time steps according to local function, which also known as rule. In details, the state at is determined by the set of neighborhoods which contain the cell itself together with the

right cell and the left cell. Thus, the next time state can be expressed as a function. Fig.1 shows the configuration of neighborhood to determine the next time state in a highlighted cell.

Figure 1:ECA Neighborhood



As each state has two possible values (0 or 1), then there will be possible combinations for neighborhoods configuration which also yield the same amount of possible output. Hence, if the neighborhood configuration is arranged in lexicographically binary order, there will be a total of distinct local rule can be created. In [1], these rules known as ECA has been studied extensively in which all rules was given a reference name that is according to decimal representation of output arrange in lexicographically order. Table 1 shows two examples of rules with its neighborhood configuration and the output state. The first row represents the neighborhood configuration of left, center, and right state. If all states at time value is 1 (the last neighborhood configuration), then the state of would be for rule 90 and for rule 150. It follows for all possible configuration. Despite the lookup table as represented in Table 1, each rule may also be represented as combination logic as follows,

$$\begin{aligned} \text{Rule 90} : q_i^{t+1} &= f(q_{i-1}^t, q_i^t, q_{i+1}^t) = q_{i-1}^t \oplus q_{i+1}^t \\ \text{Rule 150} : q_i^{t+1} &= f(q_{i-1}^t, q_i^t, q_{i+1}^t) = q_{i-1}^t \oplus q_i^t \oplus q_{i+1}^t \end{aligned} \quad \backslash * \text{ MERGEFORMAT (1.6)}$$

In this paper, the form represented in Eq.7 has a great usage compared to lookup table as represented in Table 1. Both rules are categorized as linear rule as it only involves XOR operation. If there is involvement of AND operation, the rule is a nonlinear rule.

Table 1: Lookup Table for Rule 90 and rule 150

configuration	000	001	010	011	100	101	110	111
Rule 90	0	1	0	1	1	0	1	0
Rule 150	0	1	1	0	1	0	0	1

For practicality, the CA cell array is set to be finite with length L . This implementation leads to the boundary condition problem as the state at the boundary does not have complete neighborhoods configuration. There are several types of boundary condition (BC) introduced to cater the problem. Periodic BC assume to have ring shape in which the last state is proceeds by the first state while the first state precedes by the last state. Another is null BC where it simply set zero value for both end BC (0). Some type of BC that is rarely in use such as fixed constant BC and mirror BC. Another important term in CA that is useful in this paper is uniform CA (UCA) and hybrid CA (HCA). UCA is composed of the same rule for each cell while HCA may combine more than two rules for a single cell array.

RELATED WORK

The integration of CA in cryptography algorithm is not a new as it has been integrated for decades ago. In Wolfram (1986a) and (1986b), the author propose a stream cipher using ECA rule 30 as it has been classified in class 3 ECA which has chaotic dynamic. However, it was successfully attacked by Meier & Staffelbach (1991) as the random number generated by the rule 30 has high correlation which is not a good properties for a stream cipher. Another implementation was proposed by Serra, Slater, Muzio, & Miller (1990) by using two combination of linear CA rule. Rule 90 and 150 combined together in linear hybrid cellular automata (LHCA) to generate maximum cycle of iteration. More recent work on CA integration with stream cipher can be seen in Raut & Hoe (2013) where the author combine the algorithm of CA with nonlinear feedback shift registers (NFSR). Besides stream cipher, CA also adapted in block cipher algorithm in which it become the nonlinear primitive of the algorithm or the entire cryptography scheme itself. A type of CA which is called as reversible cellular automata has been given a spotlight due to its reversible properties that is very suitable with block cipher. In Seredynski & Bouvry (2005), RCA is describe to have unique predecessor and successor in its iteration which is very ideal in block cipher to reverse the encryption process. The authors also proposed a complete algorithm of block cipher which composed of four different CA that is either UCA or RCA. Related work that depend on RCA as the main body of cryptography algorithm is presented in Kamel Mohamed (2014) where the process of encryption and decryption is done in parallel. Besides, the author also employed 2nd order RCA schemes in which the next iteration state depends on two predecessor iteration. This scheme was claimed are always reversible even the basic rule CA is not. Similar research that implement 2nd order RCA can be found in Li, Sun, Li, & Chen (2017). Besides the main algorithm, CA is no exception as the construction of substitution box (S-Box). Construction method of S-Box using CA can be classified as a heuristic method. In Szaban & Seredynski, (2008), iteration of ECA for certain rule acts as the output of the S-Box. The authors listed out the best S-Box using selected rule and number of iterations. The same author extend that idea and proposed the construction of dynamic S-Box for AES and DES in Szaban & Seredynski (2012). Low power S-Box architecture was presented in Gangadari & Ahamed (2016) where the S-Box is constructed using 2nd order programmable RCA without storing the S-Box as lookup table as has been done in conventional method. Similar research can be found in Gangadari & Rafi Ahamed, (2016). Meanwhile in Picek, Mariot, Yang, Jakobovic, & Mentens (2017), the authors presented the search of good S-Box using CA and genetic programming for S-Box size and L . The genetic programming was used to search for best CA rule in term of nonlinearity, differential uniformity, and the algebraic degree.

EXPERIMENTAL SETUP

Linear Hybrid Cellular Automata

LHCA is a type of CA that combine more than two linear rules (local function) in a single cell array . Some combination of linear rules such as rule 90 and rule 150 are able to generate full cycle of iteration as mentioned in Cattell & Muzio (1996b). Here, full cycle means all possible non-zero binary sequence of length can be generated by CA iteration based on these rules combination. Hence, for any , there will be different binary sequences that can be generated. Further, this also means the rules combination may generate the permutation of non-zero elements in decimal representation. Figure 2(a) and 2(b) show the example of full cycle and non-full cycle rule combination respectively with and null BC.

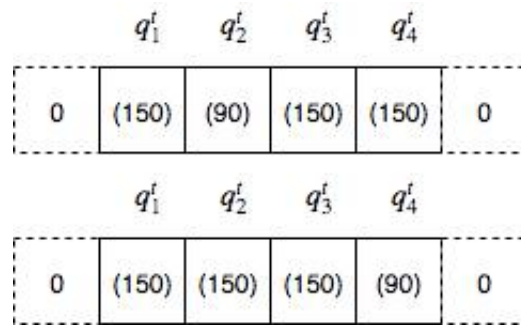


Figure 2: LHCA configuration for L=4

Figure 2 shows two different rule combinations in which Fig 2(a) has full cycle iteration while 2(b) has the opposite. To show whether it has full cycle, state transition diagram is used where each node represents one of the possible states in decimal representation. Figure 3(a) and 3(b) show the state transition diagram for configuration 2(a) and 2(b) respectively. It is clear that rule combination in 2(a) has full cycle for all non-zero elements while in 2(b), almost all elements are attracted to the limit cycle that only constitutes of seven elements.

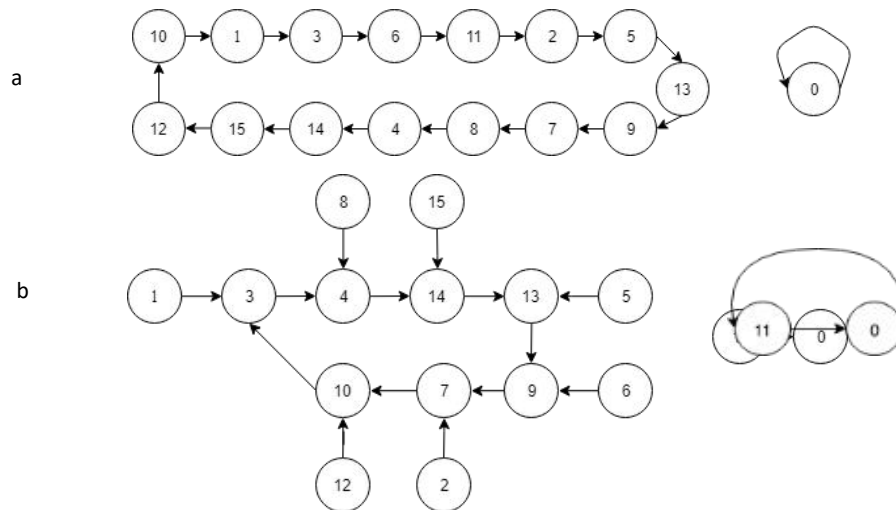


Figure 3: State transition diagram for LHCA configuration in 2(a) and 2(b) respectively

From this point onward, we present the rule combination as binary vector which is known as the control vector . Rule 90 is represented as while rule 150 as . All the information will be summarized in a control vector as where represent the rule for cell . Hence, there will be exactly different configurations that can be made including configuration of and that represent UCA of rule 90 and rule 150 respectively. At some point, we would also represent the control vector as decimal form for easier representation and reference. In previous example, it is clear that the control vector can be presented as or 5 in decimal for example in Fig.2(a).

Transition matrix and Characteristic Polynomial

In LHCA, the transition of cell array at time to can be done graphically where we construct the lattice cell and update each cell according to the rule . However, for linear rule like rule 90 and 150, this transformation can be done by constant transition matrix. The alternative is by using the transition matrix in which the iteration of cell array at time can be expressed as follows,

$$C^{t+1} = M \cdot C^t \quad \backslash * \text{MERGEFORMAT (7)}$$

where and indicates transpose vector. The transition matrix can be defined by the next state equation of every cell . Here, we refer to the combination logic in Eq.7 and example 2(a).

$$\begin{aligned} q_1^{t+1} &= q_1^t + q_2^t \\ q_2^{t+1} &= q_1^t + q_3^t \\ q_3^{t+1} &= q_2^t + q_3^t + q_4^t \\ q_4^{t+1} &= q_3^t \end{aligned}$$

The transition matrix for example in Fig.2(a) is then can be generated as the following,

$$M = \begin{bmatrix} 1 & 1 & 0 & 0 \\ 1 & 0 & 1 & 0 \\ 0 & 1 & 1 & 1 \\ 0 & 0 & 1 & 0 \end{bmatrix}$$

However, in general, the transition matrix can be constructed by setting the control vector as the diagonal of the tridiagonal matrix as shown in Eq. (9). The matrix element and determine the BC. For null BC, the value is set to 0 as in Eq.11 while for periodic BC, both elements are set to 1. Based on work found in Serra et al. (1990), the

transition matrix can be represented by characteristic polynomial and can be referred as CA polynomial. It can be calculated by using LHCA recurrence relation as follows,

$$\begin{aligned} \Delta_{-1}(x) &= 0, \\ \Delta_0(x) &= 1, \\ \Delta_k(x) &= (x + d_k)\Delta_{k-1}(x) + \Delta_{k-2}(x), \quad k \geq 1 \end{aligned} \quad \backslash * \text{ MERGEFORMAT (8)}$$

$$M = \begin{bmatrix} d_1 & 1 & 0 & \cdots & 0 & 0 & 0 \\ 1 & d_2 & 1 & \cdots & 0 & 0 & 0 \\ 0 & 1 & d_3 & \cdots & 0 & 0 & 0 \\ \vdots & \vdots & \vdots & \ddots & \vdots & \vdots & \vdots \\ 0 & 0 & 0 & \cdots & d_{L-2} & 1 & 0 \\ 0 & 0 & 0 & \cdots & 1 & d_{L-1} & 1 \\ 0 & 0 & 0 & \cdots & 0 & 1 & d_L \end{bmatrix} \quad \backslash * \text{ MERGEFORMAT (9)}$$

The following example shows the procedure of deriving characteristic polynomial of example in Fig. 2(a),

$$\begin{aligned} \Delta_{-1}(x) &= 0, \\ \Delta_0(x) &= 1, \\ \Delta_1(x) &= (x + d_1)\Delta_0(x) + \Delta_{-1}(x) = (x + 1)(1) + 0 = x + 1, \\ \Delta_2(x) &= (x + d_2)\Delta_1(x) + \Delta_0(x) = x^2 + x + 1, \\ \Delta_3(x) &= (x + d_3)\Delta_2(x) + \Delta_1(x) = x^3 + x, \\ \Delta_4(x) &= (x + d_4)\Delta_3(x) + \Delta_2(x) = x^4 + x + 1, \end{aligned} \quad \backslash * \text{ MERGEFORMAT (10)}$$

Therefore, the characteristic polynomial for example in Fig.2(a) is . This is also one of the primitive polynomials over . The polynomial is irreducible if there is no non-constant polynomial and such that . It is primitive if it has as a root that make up a set which is equal to the set of non-zero elements of Moreover, for any LHCA with full cycle, the characteristic polynomial would be the primitive polynomial. This is based on the theory presented in Cattell & Muzio (1996a), where all primitive polynomial over are CA polynomial and each primitive polynomial representing exactly two LHCA of rule 90 and rule 150.

The S-Box Construction Algorithm

Our proposed S-Box construction are based on permutation of elements generated by LHCA iteration of rule 90 and rule 150. Previous section has clearly brief that some combination of these rules may generate full cycle of iteration which constitutes the permutation of non-zero elements. The zero element however will mapped to itself.

Nevertheless, the permutation can be shifted by varying the initial condition of the iteration. Hence the value of nonlinearity, together with other security measure would also change as varying the initial condition lead to new S-Box configuration. Due to that, we have tested for all combination rule with all possible initial condition. Hence within this section, two algorithms are presented. The first algorithm are dedicated to search for all possible rule combinations that generate full cycle for . The second one is to generate S-Box from all possible initial conditions for each combination searched by the first algorithm and evaluate the S-Box using the cryptography properties as mentioned in section 2. As a result, there will be possible S-Box with different security level that can be generated where is the total number of primitive polynomials over . Both algorithms are presented as follows.

Algorithm 1: Extracting all possible rule combination

INPUT: Rule combination length , number of iterations , initial condition

OUTPUT: List of control vector that generate full cycle, LIST

```

1  Set all possible list of control vector of size
2  For from to
3      Construct matrix based on control vector
4      Set matrix for storing the iteration
5      Set
6      For from 1 to
7          Set
8          Store in
9      End
10     Set matrix for storing decimal sequence
11     For from 1 to
12         Convert into decimal representation
13         Store the decimal into
14     End
15     Sort in descending order
16     Check for permutation
17     If is a permutation
18         Write in LIST
19     End
20 End
    
```

Algorithm 1 shows the procedure to extracting all possible rule combination by testing for all possible control vector of length L . For simplicity, the initial condition is set to 0 for all i . The extracted R that able to generate full cycle is then stored for further reference in algorithm 2.

Algorithm 2: Generate and Evaluation of S-Box

INPUT: List of control vector LIST, Rule combination length

OUTPUT: Table of S-Box Nonlinearity (table) and Differential Uniformity (table)

- 1 Set empty S-Box
- 2 Set R as the first element in
- 3 Set empty matrix for storing value
- 4 **For** from 1 to L
- 5 Read R_i from LIST
- 6 **For** from 0 to $2^L - 1$
- 7 Set S
- 8 Generate the CA sequence using line 3-9 algorithm 1 with R_i and S
- 9 Convert CA iteration into decimal sequence
- 10 Store the sequence in S
- 11 Test the Nonlinearity and differential uniformity
- 12 Store S and U
- 13 **End**
- 14 **End**

Algorithm 2 shows the procedure to construct S-Box from the extracted R . All generated S-Box is then tested with cryptography properties as discussed in section 2. All results are presented in the next section together with some discussion and comparative analysis.

RESULT AND DISCUSSION

List of control vector

This section listed out all with its respective primitive polynomial extracted by algorithm 1. Based on theorem introduced in Cattell & Muzio (1996a), one primitive polynomial over represent two LHCA of rule 90 and 150. Hence, for , the number of primitive polynomial is 16 (Mullen & Panario, 2013) which resulted in 32 different possible rule combination. In Table 2, we list out all pair control vector and that represent the same primitive polynomial .

Table 2: Rule combination with its respective primitive polynomial

01100000	00000110	
11110000	00001111	
01010100	00101010	
10110100	00101101	
01101100	00110110	
10011100	00111001	
10100010	01000101	
11010010	01001011	
11011010	01011011	
10111010	01011101	
11111010	01011111	
11101110	01110111	
11001001	10010011	
11010101	10101011	
11010011	11001011	
11110111	11101111	

It can be seen from Table 2 that the rule combination pair and for any have the common relationship in which there are in reverse order of each other. As mention in Cattell & Muzio (1996a), both with the same have the same structure except the index of all cell relabeled in the opposite order. If we set the initial condition for both in opposite binary configuration, say and for and respectively, then the evolution of next time state pattern would follow to have the opposite pattern for every . This lead the generated S-Box to have the same set of coordinate function but arranged in the opposite order. As we start the iteration with invariant initial condition , this opposite pattern is not clearly appear, however all generated S-Box from both would have similar Boolean structure. It leads to another result which is the distribution of high and low S-Box for and would be the same.

Nonlinearity

Table 3 tabulate the distribution for all listed in Table 2. As mentioned before, for easier reference, we list the control vector in decimal representation with the same arrangement as in Table 2. Based on Table 3, the value of spread out ranging from the lowest of 92 up to maximum of 108. There are 16 pairs of represented by the same that have the same distribution as can be seen from the table. This is due to the reason that stated before. After all, about 65% of all constructed S-Box achieve at least and only a useful four out of 8160 constructed S-Box that achieve the value of 108. Majority of the constructed S-Box have the value of 100, 102 and 104. Only two rules combination that able to generate maximum of 108 which are and that represented as 54 and 108 in decimal notation respectively. From all generated S-Box, we have selected 10 different S-Box which show high value of . Table 4 shows in detail the value of each coordinate function for those good S-Box. The initial condition is in decimal representation. Based on that table, we have selected the generated S-Box that have the value of range from 106 to 112. The arrangement in Table 4 are made in pair, in which both S-Box have opposite arrangement of (S1 & S2, S3 & S4 and so on). Six out of 10 S-Box have maximum for at least one comparable to original AES S-Box. However, those S-Box also contain the minimum value of .

Table 3: Distribution for all

		92	94	96	98	100	102	104	106	108
6	96	0	0	0	0	80	39	121	15	0
15	240	0	0	0	0	83	76	92	4	0
42	84	31	0	49	72	55	33	10	5	0
45	180	0	0	0	0	0	56	129	70	0
54	108	0	0	0	0	0	59	129	65	2
57	156	0	0	0	0	31	128	83	13	0
69	162	0	0	0	0	93	132	28	2	0
75	210	31	0	49	40	101	21	10	3	0

91	218	0	0	0	0	83	120	50	2	0
93	186	0	0	8	0	32	151	58	6	0
95	250	0	0	0	0	141	59	53	2	0
119	238	0	0	0	0	95	84	74	2	0
147	201	0	0	8	0	57	51	96	43	0
171	213	0	0	8	55	0	45	103	44	0
203	211	0	0	0	0	90	126	31	8	0
239	247	0	0	8	0	85	75	83	4	0
Total		124	0	260	334	2052	2510	2300	576	4

Table 4: Details of selected good S-Box

Ref											Average
S1	54	72	108	108	108	108	108	108	108	108	108
S2	108	18	108	108	108	108	108	108	108	108	108
S3	54	107	108	108	108	108	108	108	108	108	108
S4	108	214	108	108	108	108	108	108	108	108	108
S5	15	17	108	112	106	108	106	106	106	106	107.25
S6	240	136	106	106	106	106	108	106	112	108	107.25
S7	15	56	106	106	106	106	108	106	112	108	107.25
S8	240	28	108	112	106	108	106	106	106	106	107.25
S9	45	90	110	108	112	108	106	106	106	106	107.75
S10	180	90	106	106	106	106	108	112	108	110	107.75

Differential Uniformity

As for differential uniformity, the value ranges from maximum 14 to minimum 8. Lowest value are more favorable in which represent almost perfect nonlinear (APN) Boolean function. Original AES S-Box achieve and known as differential 4-uniform function. Basically, each rule combination with the same would have the same value of for all possible initial condition. The following table (Table 5) shows the result of differential uniformity for each rule combination.

Table 5: for all rule combination

6	96	8
15	240	14
42	84	8
45	180	8
54	108	8
57	156	8
69	162	10
75	210	8
91	218	8
93	186	8
95	250	10
119	238	10
147	201	8
171	213	8
203	211	8
239	247	8

Algebraic Degree

We only test for algebraic degree for the selected S-Box in table 4. All S-Box from the list achieve maximum value of algebraic degree which is comparable to the one in original AES construction. The summarization of algebraic degree is shown in Table 6.

Table 6: Comparative Analysis

S-Box				Technique
S1	108	8	7	LHCA with and
S2	108	8	7	LHCA with and
S3	108	8	7	LHCA with and
S4	108	8	7	LHCA with and
S5	106	14	7	LHCA with and
S6	106	14	7	LHCA with and
S7	106	14	7	LHCA with and
S8	106	14	7	LHCA with and
S9	106	8	7	LHCA with and
S10	106	8	7	LHCA with and
AES	112	4	7	Finite Field Inversion
(Ahmad, Bhatia, & Hassan, 2015)	106	NP	NP	Ant Colony Optimization Based Scheme
(Zhang, Chen, Chen, Xu, & Hu, 2018)	108	10	7	I-Ching operator
(Ye & Zhimao, 2018)	104	10	7	Six-Dimensional Fractional Lorenz-Duffing System
(Ahmed, Zolkipli, & Ahmad, 2018)	106	10	7	Firefly algorithm and Discrete chaotic map
(Gangadari & Ahamed, 2016)	108	18	7	Programmable 2 nd order RCA

NP-Not Provided

Comparative Analysis

Finally, we conduct a comparative analysis in order to compare our S-Box performance with other construction. We gather the work of S-Box construction using various of work including CA and other heuristic methods. Table 6 list out selected work for comparison in term of nonlinearity , differential uniformity and the algebraic degree. From the table, our proposed method able to generate S-Box with higher nonlinearity compared to another construction. However, some of the constructed S-Box may have lower security as the value of differential uniformity is high compared to the optimum one. In term of algebraic degree, the proposed method able to generate S-Box with optimum value of algebraic degree.

CONCLUSION

Our new proposed S-Box generally are based on hybrid CA that produced full cycle of iteration. The construction presented in this paper manage to achieve the value of nonlinearity with maximum of 108 and minimum of 92. Besides, the method also manage to generate S-Box with differential uniformity of 8 and maximum algebraic degree of 7. Compared to other method in the class, this method may have better performance S-Box in term of maximum nonlinearity as we can detect single coordinate function with maximum value of 112, that is comparable to AES S-Box. In the future, this method can be extend to other size of S-Box and with better planning and algorithm, dynamic S-Box could also be implemented using the proposed methods. This is due to the variability of initial condition and control vector together with simplest algorithm compared to original one that implement finite field inversion.

ACKNOWLEDGEMENT

The authors would like to express special thanks to Ministry of Education Malaysia for supporting and financing this research project under the Transdisciplinary Research Grant Scheme (TRGS/FKAB/50216/59). The author would also thanks to anonymous reviewers for their helpful comment and suggestion.

REFERENCES

Ahmad, M., Bhatia, D., & Hassan, Y. (2015). A Novel Ant Colony Optimization Based Scheme for Substitution Box Design. *Procedia - Procedia Computer Science*, 57, 572–580.

Ahmed, H. A., Zolkipli, M. F., & Ahmad, M. (2018). A novel efficient substitution-box design based on firefly algorithm and discrete chaotic map. *Neural Computing and Applications*, 3, 1–10.

Bertoni, G., Daemen, J., Peeters, M., Assche, G. V. Van, Guido, B., Joan, D., ... Gilles, V. A. (2011). The keccak reference. *Submission to NIST (Round 3)*, 1–14.

Biham, E., & Shamir, A. (1990). Differential Cryptanalysis of DES-like Cryptosystems. In *Advances in Cryptology - CRYPTO '90, 10th Annual International Cryptology Conference, Santa Barbara, California, USA, August 11-15, 1990, Proceedings* (Vol. 537, pp. 2–21).

Cattell, K., & Muzio, J. C. (1996a). Analysis of One-Dimensional Linear Hybrid Cellular Automata over $GF(q)$. *IEEE Transactions on Computers*, 7(July 1996).

Cattell, K., & Muzio, J. C. (1996b). Synthesis of one-dimensional linear hybrid cellular automata. *IEEE Transactions on Computer-Aided Design of Integrated Circuits and Systems*, 15(3), 325–335.

Gangadari, B. R., & Ahamed, S. R. (2016). Low Power S-Box Architecture for AES Algorithm using Programmable Second Order Reversible Cellular Automata: An Application to WBAN. *Journal of Medical Systems*, 40(12).

Gangadari, B. R., & Rafi Ahamed, S. (2016). Design of cryptographically secure AES like S-Box using second-order reversible cellular automata for wireless body area network applications. *Healthcare Technology Letters*, 3(3), 177–183.

Kamel Mohamed, F. (2014). A parallel block-based encryption schema for digital images using reversible cellular automata. *Engineering Science and Technology, an International Journal*, 17(2), 85–94.

Li, K., Sun, M., Li, L., & Chen, J. (2017). Image Encryption Algorithms Based on Non-uniform Second-Order Reversible Cellular Automata with Balanced Rules. In *Intelligent Computing Theories and Application. ICIC 2017. Lecture Notes in Computer Science* (Vol. 10362, pp. 445–455). Springer, Cham.

Meier, W., & Staffelbach, O. (1991). Analysis of Pseudo Random Sequence Generated by Cellular Automata.

Mullen, G. L., & Panario, D. (2013). *Handbook of finite fields*. CRC Press.

Picek, S., Mariot, L., Yang, B., Jakobovic, D., & Mentens, N. (2017). Design of S-boxes defined with cellular automata rules. *ACM International Conference on Computing Frontiers 2017, CF 2017*, 409–414.

Raut, L., & Hoe, D. H. K. (2013). Stream cipher design using cellular automata implemented on FPGAs. *45th Southeastern Symposium on System Theory*, 146–149.

Seredynski, M., & Bouvry, P. (2005). Block Cipher based on Reversible Cellular Automata. *New Gener Comput*, 23(3), 245–258.

Serra, M., Slater, T., Muzio, J. C., & Miller, D. M. (1990). The Analysis of One-Dimensional Linear Cellular Automata and Their Aliasing Properties. *IEEE Transactions on Computer-Aided Design of Integrated Circuits and Systems*, 9(7), 767–778.

Szaban, M., & Seredynski, F. (2008). Application of cellular automata to create S-box functions. *IPDPS Miami 2008 - Proceedings of the 22nd IEEE International Parallel and Distributed Processing Symposium, Program and CD-ROM*.

Szaban, M., & Seredynski, F. (2012). Dynamic cellular automata-based S-boxes. *Lecture Notes in Computer Science (Including Subseries Lecture Notes in Artificial Intelligence and Lecture Notes in Bioinformatics)*, 6927 LNCS(PART 1), 184–191.

Wolfram, S. (1986a). Cryptography with Cellular Automata. *Lecture Notes in Computer Science (Including Subseries Lecture Notes in Artificial Intelligence and Lecture Notes in Bioinformatics)*.

Wolfram, S. (1986b). *Random sequence generation by cellular automata. Advances in Applied Mathematics (Vol. 7)*.

Wolfram, S. (2002). *A New Kind of Science*. Champaign: Wolfram media.

Ye, T., & Zhimao, L. (2018). Chaotic S-box: six-dimensional fractional Lorenz–Duffing chaotic system and O-shaped path scrambling. *Nonlinear Dynamics*, (2).

Zhang, T., Chen, C. L. P., Chen, L., Xu, X., & Hu, B. (2018). Design of Highly Nonlinear Substitution Boxes Based on I-Ching Operators. *IEEE Transactions on Cybernetics*, PP, 1–10.